

Design Criteria for SGD Preconditioners: Local Conditioning, Noise Floors, and Basin Stability

Anonymous authors
Paper under double-blind review

Abstract

1 Stochastic Gradient Descent (SGD) often slows in the late stage of training due to anisotropic
 2 curvature and gradient noise. We analyze preconditioned SGD in the geometry induced
 3 by a symmetric positive definite matrix \mathbf{M} . Our bounds make explicit how both the
 4 convergence rate and the stochastic noise floor depend on \mathbf{M} . For nonconvex objectives, we
 5 establish a basin-stability guarantee in a local \mathbf{M} -metric neighborhood around a minimizer
 6 set: under local smoothness and a local PL condition, we give an explicit lower bound on the
 7 probability that the iterates remain in the basin up to a time horizon. This perspective is
 8 particularly relevant in Scientific Machine Learning (SciML), where reaching small training
 9 losses under stochastic updates is closely tied to physical fidelity, numerical stability, and
 10 constraint satisfaction. Our framework covers both diagonal/adaptive and curvature-aware
 11 preconditioners and yields a practical criterion: choose \mathbf{M} to improve local conditioning
 12 while attenuating noise in the \mathbf{M}^{-1} -norm. Experiments on a quadratic diagnostic and three
 13 SciML benchmarks support the predicted rate–floor behavior.

1 Introduction

15 Stochastic Gradient Descent (SGD) has long been the workhorse of large-scale machine learning. Since
 16 its early application to multilayer perceptrons in the 1960s (Amari, 1967), its simplicity, scalability, and
 17 low per-iteration cost have made it a popular optimizer for deep learning models (Bottou et al., 2018).
 18 Classical convergence theory for SGD under noisy gradients typically guarantees a sublinear rate of $\mathcal{O}(1/k)$
 19 under convexity and smoothness assumptions (Robbins & Monro, 1951; Blum, 1954). The theory for SGD
 20 convergence under various combinations of conditions is well studied and documented in Garrigos & Gower
 21 (2024); Khaled & Richtárik (2023), and Francis Bach (2024).

22 Recent theoretical developments have established *linear convergence* for SGD under stronger conditions, such
 23 as strong convexity, smoothness, and bounded noise (Bottou et al., 2018). When the loss F is c -strongly
 24 convex, has L -Lipschitz gradients, and the learning rate α satisfies $\alpha \leq \mu/(LK_G)$, the iterates \mathbf{w}_k satisfy

$$\mathbb{E}[F(\mathbf{w}_k) - F_*] \leq (1 - \alpha c \mu)^{k-1} \left(F(\mathbf{w}_1) - F_* - \frac{\alpha L K}{2c\mu} \right) + \frac{\alpha L K}{2c\mu}, \quad (1)$$

25 where μ , K , and K_G are constants associated with the stochastic gradients (defined in Assumptions 9–11),
 26 and let \mathbf{w}^* denote the unique minimizer and $F_* := F(\mathbf{w}^*)$ the optimal value. Eq. (1) highlights two late-stage
 27 drivers: a linear contraction factor $1 - \alpha c \mu$ and a stochastic error floor

$$\frac{\alpha L K}{2c\mu} = \frac{\alpha}{2\mu} \kappa K,$$

28 where $\kappa := \frac{L}{c}$ is the (Euclidean) condition number associated with curvature. For any admissible α , the floor
 29 scales with κ and K , while the contraction depends on the product $\alpha c \mu$.

30 Many successful optimizers can be viewed as *preconditioned variants of SGD*. Adaptive methods such as
 31 Adagrad (Duchi et al., 2011), Adam (Kingma & Ba, 2017), and RMSProp (Hinton, 2014), structured

32 second-order approaches including Shampoo (Gupta et al., 2018), K-FAC (Martens & Grosse, 2015; Ishikawa
 33 & Karakida, 2024), and Sophia (Liu et al., 2024), as well as quasi-Newton methods like L-BFGS (Liu &
 34 Nocedal, 1989; Chen et al., 2014), all apply a linear transformation to the gradient that reshapes both
 35 curvature and gradient noise. From this perspective, their empirical effectiveness indicates that late-stage
 36 optimization is influenced not only by the choice of learning rates, but also by how the preconditioning alters
 37 local conditioning and the geometry of stochastic noise. Despite their widespread use, however, there is still
 38 no unified theoretical framework that identifies which properties of a preconditioner determine the late-stage
 39 convergence rate and the attainable noise floor.

Motivated by this perspective, we study the preconditioned SGD update in the following form

$$\mathbf{w}_{k+1} = \mathbf{w}_k - \alpha_k \mathbf{M}^{-1} g(\mathbf{w}_k, \xi_k), \quad (2)$$

40 where $\mathbf{M} \succ 0$ is a symmetric positive definite (SPD) matrix that defines the geometry in which both curvature
 41 and noise are measured, $g(\mathbf{w}_k, \xi_k) = \nabla_{\mathbf{w}} F_k(\mathbf{w})$ is the stochastic gradient, α_k is the learning rate, ξ_k is an i.i.d.
 42 sample drawn at iteration k . The standard (vanilla) SGD update is recovered when $\mathbf{M} = \mathbf{I}$. Our goal is not
 43 to propose a new optimizer, but to provide a principled framework to analyze and compare preconditioners
 44 in the late stage of training.

45 **Main contributions** We investigate how preconditioning influences the late-stage behavior of SGD within
 46 a well-behaved basin of the loss surface. By analyzing preconditioned SGD in the \mathbf{M} -induced geometry, we
 47 show how rescaling the gradient affects both the convergence rate and the attainable noise floor, and we
 48 derive criteria that clarify which properties of a preconditioner matter in the late stage of training.

49 **1. Preconditioned SGD in the strongly convex baseline.** We extend the classical “linear rate
 50 + noise floor” theory for SGD to updates preconditioned by a fixed SPD matrix \mathbf{M} . The resulting
 51 bounds show that late-stage behavior is controlled by (i) an effective conditioning in the \mathbf{M} -geometry
 52 and (ii) the preconditioned gradient-noise level; the attainable error floor scales with their *product*.
 53 Since admissible constant stepsizes are limited by \mathbf{M} -smoothness, improved conditioning allows larger
 54 stepsizes and hence faster contraction. With diminishing stepsizes, we obtain an $\mathcal{O}(1/k)$ rate.

55 **2. Local nonconvex regime with basin stability.** Under a local \mathbf{M} -PL condition and local
 56 smoothness, we establish late-stage convergence guarantees inside a well-behaved basin around a
 57 minimizer set, again with an explicit rate–floor structure. In addition, we provide a basin-stability
 58 bound that lower-bounds the probability of remaining in the basin up to a horizon.

59 **3. Design criteria and empirical evidence.** Our theory yields a simple design principle: choose \mathbf{M}
 60 to improve local conditioning while attenuating noise in the \mathbf{M}^{-1} -norm; the attainable late-stage
 61 floor tracks their product. We validate this mechanism on (i) a quadratic diagnostic where the
 62 relevant constants can be computed in closed form, and (ii) three SciML benchmarks where late-stage
 63 behavior is strongly tied to final accuracy.

64 While late-stage convergence is broadly relevant, it is especially important in SciML. Here, training losses
 65 encode physically meaningful quantities (e.g., PDE residuals, boundary conditions, stability). Unlike standard
 66 ML tasks where moderate error may still be acceptable, small reductions in the final loss can determine whether
 67 solutions conserve invariants, remain stable over long horizons, or meet scientific accuracy requirements. In
 68 this setting, the optimizer’s asymptotic behavior—and particularly the final noise floor—directly governs
 69 physical fidelity (Zhang et al., 2024).

70 2 Related work

71 Recent work has advanced the theoretical understanding of preconditioned and adaptive variants of SGD
 72 under various structural and noise assumptions. Koren et al. (2022) showed that preconditioned SGD
 73 achieves a rate of $\mathcal{O}(1/\sqrt{k})$ for general stochastic convex optimization, though convergence can stagnate in
 74 the presence of persistent gradient noise. Faw et al. (2022) further established that adaptive SGD attains

75 an order-optimal $\tilde{\mathcal{O}}(1/\sqrt{k})$ rate for nonconvex smooth objectives under affine variance conditions, without
 76 requiring bounded gradients or finely tuned learning rates. More recently, Attia & Koren (2023) derived
 77 high-probability guarantees of $\tilde{\mathcal{O}}(1/k + \sigma_0/\sqrt{k})$ for adaptive methods in both convex and nonconvex settings,
 78 relaxing the need for strong smoothness or prior parameter knowledge.

79 These results primarily address *global* convergence behavior across general problem classes. In contrast, our
 80 analysis focuses on the *asymptotic regime*—the late stage of training where iterates lie within a well-behaved
 81 basin around a local minimizer and optimization progress is limited by curvature anisotropy and gradient
 82 noise. In this regime, we show that both the convergence rate and the noise floor of the preconditioned SGD
 83 are determined by curvature and variance quantities measured in the preconditioned geometry. This local,
 84 geometry-aware viewpoint clarifies why curvature-informed preconditioners and adaptive algorithms yield
 85 faster and more stable late-stage convergence.

86 Other techniques such as batch normalization (Lange et al., 2022) and weight decay (Loshchilov & Hutter,
 87 2017; Barrett & Dherin, 2020) can also be interpreted as implicit forms of preconditioning, though they operate
 88 through different regularization mechanisms. For comprehensive surveys of explicit preconditioned SGD and
 89 related adaptive methods, we refer the reader to Ye (2024). **Beyond convergence rates, preconditioning has**
 90 **also been studied as an implicit regularization that may affect generalization** (ichi Amari et al., 2021).

91 3 Preconditioned SGD convergence analysis

92 We first analyze the globally strongly convex case as a *baseline* to make the role of the preconditioned geometry
 93 explicit. Although this setting is rarely realized in deep learning, it reveals the essential mechanism through
 94 which preconditioning affects convergence. The analysis shows how curvature and noise floor transform
 95 under a change of metric, providing a principled way to compare different choices of \mathbf{M} . This also lays the
 96 groundwork for the local nonconvex analysis in Section 3.2, where \mathbf{M} influences both basin size and stability.

97 3.1 Convergence in the globally strongly convex setting

98 We establish convergence guarantees for preconditioned SGD when the objective is globally strongly convex.
 99 This simplified setting allows for a transparent analysis of how a preconditioner reshapes both the effective
 100 curvature and the gradient noise. While the derivations parallel the Euclidean case, expressing them in the
 101 \mathbf{M} -induced geometry makes the dependence on the preconditioner explicit and lays the groundwork for the
 102 more general nonconvex results to follow.

103 **Curvature assumptions.** Preconditioning redefines smoothness and strong convexity through effective
 104 constants (\hat{L}, \hat{c}) measured in the \mathbf{M} -induced norm.

105 **Assumption 1** (\mathbf{M} -strong convexity). $F: \mathbb{R}^d \rightarrow \mathbb{R}$ is \mathbf{M} -strongly convex: there exists $\hat{c} > 0$ such that

$$F(\bar{\mathbf{w}}) \geq F(\mathbf{w}) + \nabla F(\mathbf{w})^\top (\bar{\mathbf{w}} - \mathbf{w}) + \frac{1}{2} \hat{c} \|\bar{\mathbf{w}} - \mathbf{w}\|_{\mathbf{M}}^2, \quad \forall \bar{\mathbf{w}}, \mathbf{w} \in \mathbb{R}^d.$$

106 **Assumption 2** (\mathbf{M} -Lipschitz gradient). ∇F is \mathbf{M} -Lipschitz with constant $\hat{L} > 0$:

$$\|\nabla F(\bar{\mathbf{w}}) - \nabla F(\mathbf{w})\|_{\mathbf{M}^{-1}} \leq \hat{L} \|\bar{\mathbf{w}} - \mathbf{w}\|_{\mathbf{M}}, \quad \forall \bar{\mathbf{w}}, \mathbf{w} \in \mathbb{R}^d.$$

107 These conditions are direct analogues of the Euclidean definitions. Writing $\mathbf{M}^{-1} = \mathbf{P}\mathbf{P}^\top$ gives the spectral
 108 characterization:

109 **Lemma 3.1.** Let F be twice differentiable and $\mathbf{M}^{-1} = \mathbf{P}\mathbf{P}^\top$. Then: (i) ∇F is \mathbf{M} -Lipschitz with constant
 110 $\hat{L} \iff$ all eigenvalues of $\mathbf{P}^\top \nabla^2 F(\mathbf{w}) \mathbf{P}$ are $\leq \hat{L}$; (ii) F is \mathbf{M} -strongly convex with constant $\hat{c} \iff$ all
 111 eigenvalues of $\mathbf{P}^\top \nabla^2 F(\mathbf{w}) \mathbf{P}$ are $\geq \hat{c}$.

112 Hence, preconditioning improves the effective condition number whenever $\hat{L}/\hat{c} < L/c$.

113 **Noise assumptions.** We measure the first and second moments of the stochastic gradient in the \mathbf{M}^{-1} -norm.
 114 Specifically, holding \mathbf{w}_k fixed, we define the variance with respect to the sampling of ξ_k by

$$\mathbb{V}_{\xi_k}[g(\mathbf{w}_k, \xi_k), \|\cdot\|_{\mathbf{M}^{-1}}] := \mathbb{E}_{\xi_k} [\|g(\mathbf{w}_k, \xi_k)\|_{\mathbf{M}^{-1}}^2] - \|\mathbb{E}_{\xi_k}[g(\mathbf{w}_k, \xi_k)]\|_{\mathbf{M}^{-1}}^2. \quad (3)$$

Assumption 3 (Moment bounds in \mathbf{M}^{-1}). *For the iterates of (2), there exist constants $\mu_G \geq \mu > 0$, $K \geq 0$, and $K_V \geq 0$ such that, for all k ,*

$$\langle \nabla F(\mathbf{w}_k), \mathbb{E}_{\xi_k}[g(\mathbf{w}_k, \xi_k)] \rangle_{\mathbf{M}^{-1}} \geq \mu \|\nabla F(\mathbf{w}_k)\|_{\mathbf{M}^{-1}}^2, \quad (4)$$

$$\|\mathbb{E}_{\xi_k}[g(\mathbf{w}_k, \xi_k)]\|_{\mathbf{M}^{-1}} \leq \mu_G \|\nabla F(\mathbf{w}_k)\|_{\mathbf{M}^{-1}}, \quad (5)$$

$$\mathbb{V}_{\xi_k}[g(\mathbf{w}_k, \xi_k), \|\cdot\|_{\mathbf{M}^{-1}}] \leq K + K_V \|\nabla F(\mathbf{w}_k)\|_{\mathbf{M}^{-1}}^2. \quad (6)$$

115 We call K the *preconditioned noise level* because the variance in the \mathbf{M}^{-1} -norm satisfies

$$\mathbb{V}_{\xi}[g(\mathbf{w}, \xi), \|\cdot\|_{\mathbf{M}^{-1}}] = \text{tr}(\mathbf{M}^{-1} \Sigma(\mathbf{w})),$$

116 where $\Sigma(\mathbf{w}) := \text{Cov}(g(\mathbf{w}, \xi) \mid \mathbf{w})$. In the stationary case $\Sigma(\mathbf{w}) \equiv \Sigma$, we have the fixed $\text{tr}(\mathbf{M}^{-1} \Sigma)$. More
117 generally, on a region containing the iterates it is natural to choose $K \geq \sup_{\mathbf{w}} \text{tr}(\mathbf{M}^{-1} \Sigma(\mathbf{w}))$, so K is a
118 uniform baseline for the preconditioned noise.

119 Under these assumptions we obtain the usual linear and sublinear rates, but with constants that depend
120 explicitly on the preconditioned geometry.

121 **Theorem 3.2.** *Under Assumptions 1–3 (with $F_{\min} = F_*$), suppose (2) uses a fixed learning rate $\alpha_k = \bar{\alpha}$ with*

$$0 < \bar{\alpha} \leq \frac{\mu}{\hat{L} K_G} \quad \text{where } K_G = K_V + \mu_G^2 \geq \mu^2 > 0.$$

Then, for all $k \in \mathbb{N}$,

$$\mathbb{E}[F(\mathbf{w}_k) - F_*] \leq \frac{\bar{\alpha} \hat{L} K}{2 \hat{c} \mu} + (1 - \bar{\alpha} \hat{c} \mu)^{k-1} \left(F(\mathbf{w}_1) - F_* - \frac{\bar{\alpha} \hat{L} K}{2 \hat{c} \mu} \right) \xrightarrow{k \rightarrow \infty} \frac{\bar{\alpha} \hat{L} K}{2 \hat{c} \mu}. \quad (7)$$

122 Theorem 3.2 shows that, with a fixed learning rate $\bar{\alpha}$, preconditioned SGD contracts linearly with factor
123 $1 - \bar{\alpha} \hat{c} \mu$ and converges to an asymptotic floor

$$\frac{\bar{\alpha} \hat{L} K}{2 \hat{c} \mu} = \frac{\bar{\alpha}}{2 \mu} \left(\frac{\hat{L}}{\hat{c}} \right) K.$$

124 Thus, the floor factorizes into an *effective condition number* \hat{L}/\hat{c} and a *preconditioned noise level* K . In the
125 late stage of training, we have $F(\mathbf{w}_k) - F_* = \mathcal{O}(\bar{\alpha} K)$ and $\|\nabla F(\mathbf{w}_k)\|_{\mathbf{M}^{-1}}^2 = \mathcal{O}(\bar{\alpha} K)$. Substituting into the
126 variance bound (6) gives

$$\mathbb{V}_{\xi_k}[g(\mathbf{w}_k, \xi_k), \|\cdot\|_{\mathbf{M}^{-1}}] \leq K + \mathcal{O}(\bar{\alpha} K),$$

127 so for small $\bar{\alpha}$ the variance is dominated by the baseline K term.

128 Moreover, since $\mathbb{V}_{\xi}[g(\mathbf{w}, \xi), \|\cdot\|_{\mathbf{M}^{-1}}] = \text{tr}(\mathbf{M}^{-1} \Sigma(\mathbf{w}))$, we may view K as an upper baseline for the precondi-
129 tioned noise $\text{tr}(\mathbf{M}^{-1} \Sigma(\mathbf{w}))$ along the late-stage trajectory. Preconditioning reduces this baseline through its
130 effect on $\text{tr}(\mathbf{M}^{-1} \Sigma(\mathbf{w}))$; choosing \mathbf{M} to attenuate high-variance directions lowers this trace and thus lowers
131 the effective noise floor.

132 **Theorem 3.3.** *Under Assumptions 1–3 (with $F_{\min} = F_*$), suppose (2) uses $\alpha_k = \beta/(\gamma + k)$ with $\beta > \frac{1}{\hat{c} \mu}$
133 and $\gamma > 0$ chosen so that $\alpha_1 \leq \mu/(\hat{L} K_G)$. Then, for all $k \in \mathbb{N}$,*

$$\mathbb{E}[F(\mathbf{w}_k) - F_*] \leq \frac{\nu}{\gamma + k}, \quad \nu := \max \left\{ \frac{\beta^2 \hat{L} K}{2(\beta \hat{c} \mu - 1)}, (\gamma + 1)(F(\mathbf{w}_1) - F_*) \right\}. \quad (8)$$

134 With diminishing learning rates, the noise floor vanishes and Theorem 3.3 shows that preconditioned SGD
135 attains the optimal $\mathcal{O}(1/k)$ rate. Preconditioning no longer changes the rate itself—it always decays like
136 $1/k$ —but it directly influences the leading constant ν which has the same structure as the fixed-learning-rate
137 floor: an effective condition number \hat{L}/\hat{c} multiplied by the preconditioned noise level K . Thus even when
138 the noise floor disappears, late-stage performance is still governed by the same metric-dependent quantities
139 (\hat{L}, \hat{c}, K). Consequently, effective preconditioners must again balance curvature alignment (to reduce \hat{L}/\hat{c})
140 with noise attenuation (to reduce K), improving both the asymptotic constants in the $\mathcal{O}(1/k)$ regime.

141 **3.2 Local convergence in the nonconvex setting**

142 The empirical loss $F(\mathbf{w})$ over network parameters is typically *nonconvex*, and its local geometry near
 143 minimizers is rarely strictly convex. Empirical studies show that trained models often converge to regions
 144 that are flat in many directions and exhibit highly degenerate curvature—manifested as a cluster of very
 145 small or near-zero eigenvalues in the Hessian—arising from overparameterization, symmetries, and parameter
 146 non-identifiability (Sagun et al., 2018; Ghorbani et al., 2019). Despite this degeneracy, the optimization
 147 dynamics remain structured: iterates contract along directions with significant curvature while the loss
 148 changes little along flat directions. To describe this late-stage regime without assuming strong convexity, we
 149 impose a *local Polyak–Łojasiewicz (PL)* condition (Chan, 1979; Karimi et al., 2016) in the \mathbf{M} –geometry, which
 150 enforces gradient domination only in informative directions and tolerates flat or weakly curved subspaces.
 151 This flat-tolerant formulation provides a natural framework to study how preconditioning reshapes local
 152 curvature and noise, governing contraction rates, asymptotic error floors, and stability during the final phase
 153 of optimization.

154 **Additional local assumptions.** Fix an SPD matrix \mathbf{M} and an open neighborhood $\mathcal{U} \subset \mathbb{R}^d$. Assume the
 155 local minimizer set

$$\mathcal{S} := \arg \min_{\mathbf{w} \in \mathcal{U}} F(\mathbf{w}) \neq \emptyset, \quad F_* := \min_{\mathbf{w} \in \mathcal{U}} F(\mathbf{w}) = F(\mathbf{s}) \text{ for any } \mathbf{s} \in \mathcal{S}.$$

156 Write $\|x\|_{\mathbf{M}} := (x^\top \mathbf{M} x)^{1/2}$ and $\text{dist}_{\mathbf{M}}(\mathbf{w}, \mathcal{S}) := \inf_{\mathbf{s} \in \mathcal{S}} \|\mathbf{w} - \mathbf{s}\|_{\mathbf{M}}$. For radii $0 < r < r_+$, define the \mathbf{M} –metric
 157 neighborhoods

$$\mathcal{N}_r := \{\mathbf{w} : \text{dist}_{\mathbf{M}}(\mathbf{w}, \mathcal{S}) \leq r\}, \quad \mathcal{N}_{r_+} := \{\mathbf{w} : \text{dist}_{\mathbf{M}}(\mathbf{w}, \mathcal{S}) \leq r_+\} \subseteq \mathcal{U}.$$

158 We assume the following conditions hold on \mathcal{N}_r (for the iterates) and on \mathcal{N}_{r_+} (for the exit bound).

159 **Assumption 4** (Local \mathbf{M} –PL on \mathcal{N}_r). *There exists $\hat{\mu}_{\text{PL}} > 0$ such that, for all $\mathbf{w} \in \mathcal{N}_r$,*

$$2\hat{\mu}_{\text{PL}}(F(\mathbf{w}) - F_*) \leq \|\nabla F(\mathbf{w})\|_{\mathbf{M}^{-1}}^2.$$

160 **Assumption 5** (Local \mathbf{M} –Lipschitz gradient on a convex neighborhood of \mathcal{N}_{r_+}). *There exists an open convex
 161 set \mathcal{V} with $\mathcal{N}_{r_+} \subset \mathcal{V} \subseteq \mathcal{U}$ and a constant $\hat{L} > 0$ such that, for all $\bar{\mathbf{w}}, \mathbf{w} \in \mathcal{V}$,*

$$\|\nabla F(\bar{\mathbf{w}}) - \nabla F(\mathbf{w})\|_{\mathbf{M}^{-1}} \leq \hat{L} \|\bar{\mathbf{w}} - \mathbf{w}\|_{\mathbf{M}}.$$

162 **Assumption 6** (Local stochastic gradient conditions on \mathcal{N}_r). *Let (\mathcal{F}_k) denote the natural filtration and set
 163 $g_k := g(\mathbf{w}_k, \xi_k)$. There exist constants $\mu \in (0, 1]$, $K_G \geq 0$, and $K \geq 0$ such that, for every k with $\mathbf{w}_k \in \mathcal{N}_r$,*

$$\langle \nabla F(\mathbf{w}_k), \mathbb{E}[g_k | \mathcal{F}_k] \rangle_{\mathbf{M}^{-1}} \geq \mu \|\nabla F(\mathbf{w}_k)\|_{\mathbf{M}^{-1}}^2, \quad \mathbb{E}[\|g_k\|_{\mathbf{M}^{-1}}^2 | \mathcal{F}_k] \leq K_G \|\nabla F(\mathbf{w}_k)\|_{\mathbf{M}^{-1}}^2 + K.$$

164 **Assumption 7** (Local quadratic growth (QG) on \mathcal{N}_{r_+}). *There exists $\alpha_{\text{QG}} > 0$ such that, for all $\mathbf{w} \in \mathcal{N}_{r_+}$,*

$$F(\mathbf{w}) - F_* \geq \frac{\alpha_{\text{QG}}}{2} \text{dist}_{\mathbf{M}}(\mathbf{w}, \mathcal{S})^2.$$

165

166 **Assumption 8** (Controlled one-step overshoot on \mathcal{N}_r). *Fix radii $0 < r < r_+$ and a horizon $T \geq 1$, and set
 167 $\Delta := r_+ - r$. There exist deterministic numbers $(\delta_k)_{k=1}^{T-1}$ with $\delta_k \in [0, 1)$ such that for every $k \leq T - 1$,*

$$\mathbf{1}_{\{\mathbf{w}_k \in \mathcal{N}_r\}} \alpha_k^2 \mathbb{E}[\|g_k\|_{\mathbf{M}^{-1}}^2 | \mathcal{F}_k] \leq \delta_k \Delta^2 \quad \text{a.s.}$$

168 Lemma 3.4 gives the one-step containment probability implied by Assumption 8.

169

170 **Lemma 3.4** (Containment probability implied by Assumption 8). *Under Assumption 8, for every $k \leq T - 1$,*

$$\mathbf{w}_k \in \mathcal{N}_r \implies \mathbb{P}(\mathbf{w}_{k+1} \in \mathcal{N}_{r_+} | \mathcal{F}_k) \geq 1 - \delta_k.$$

171 These local assumptions are the basin-restricted analogue of the global conditions in Section 3.1. The local
 172 **M**-PL condition replaces global strong convexity by a *gradient-domination* inequality in the **M**-metric: it
 173 enforces curvature only in directions that drive descent while permitting flat or weakly curved directions.
 174 The local **M**-Lipschitz gradient assumption on a convex neighborhood $\mathcal{V} \supset \mathcal{N}_{r_+}$ provides a quadratic upper
 175 model along any update segment that stays in \mathcal{V} :

$$F(\bar{\mathbf{w}}) \leq F(\mathbf{w}) + \nabla F(\mathbf{w})^\top (\bar{\mathbf{w}} - \mathbf{w}) + \frac{\hat{L}}{2} \|\bar{\mathbf{w}} - \mathbf{w}\|_{\mathbf{M}}^2.$$

176 In our finite-horizon analysis, this condition is invoked only on trajectories for which the iterates (and hence
 177 the corresponding update segments, by convexity) remain inside \mathcal{V} up to time T .

178 The local stochastic gradient condition (Assumption 6) mirrors the global moment bounds in Assumption 3,
 179 but is only required to hold when $\mathbf{w}_k \in \mathcal{N}_r$. It imposes a first-moment alignment condition and a *second-*
 180 *moment* bound in the \mathbf{M}^{-1} -norm, which is the natural scale for preconditioned updates. The local QG
 181 condition ensures that the objective grows at least quadratically with $\text{dist}_{\mathbf{M}}(\mathbf{w}, \mathcal{S})$ near the basin boundary—a
 182 property that holds, for example, when curvature is positive in normal directions—and it supplies the barrier
 183 needed in the optional-stopping/exit-time argument.

184 **Assumption 8** controls rare one-step overshoots from the inner basin \mathcal{N}_r to outside the enlarged neighborhood
 185 \mathcal{N}_{r_+} . When $\mathbf{w}_k \in \mathcal{N}_r$, the preconditioned update moves a distance

$$\|\mathbf{w}_{k+1} - \mathbf{w}_k\|_{\mathbf{M}} = \alpha_k \|g_k\|_{\mathbf{M}^{-1}}.$$

186 Since $\text{dist}_{\mathbf{M}}(\mathbf{w}_k, \mathcal{S}) \leq r$ on \mathcal{N}_r , the triangle inequality implies that $\mathbf{w}_{k+1} \notin \mathcal{N}_{r_+}$ can occur only if $\alpha_k \|g_k\|_{\mathbf{M}^{-1}} >$
 187 Δ with $\Delta := r_+ - r$. Assumption 8 bounds the conditional second moment of $\|g_k\|_{\mathbf{M}^{-1}}$ relative to Δ ; therefore,
 188 by Markov's inequality,

$$\mathbb{P}(\mathbf{w}_{k+1} \notin \mathcal{N}_{r_+} \mid \mathcal{F}_k) \leq \delta_k \quad \text{whenever } \mathbf{w}_k \in \mathcal{N}_r.$$

189 Together, these assumptions describe a local regime that accommodates moderate nonconvexity and flatness
 190 while still providing sufficient structure for quantitative finite-horizon convergence and stability guarantees
 191 under stochastic gradients.

192 **Theorem 3.5** (Convergence in a local basin up to a finite horizon). *Fix radii $0 < r < r_+$ and a horizon
 193 $T \geq 1$, and let*

$$\tau := \inf\{k \geq 1 : \mathbf{w}_k \notin \mathcal{N}_r\}, \quad \Omega_T := \{\tau > T\}.$$

194 *Assume: (i) Assumptions 4 and 6 hold on \mathcal{N}_r ; (ii) Assumption 5 holds on a convex set \mathcal{V} with $\mathcal{N}_{r_+} \subset \mathcal{V} \subseteq \mathcal{U}$;
 195 (iii) Assumption 7 holds on \mathcal{N}_{r_+} ; (iv) Assumption 8 holds with horizon T and failure probabilities $(\delta_k)_{k=1}^{T-1}$;
 196 and (v) the conditional-moment version of Assumption 6 holds on Ω_T (i.e., the first/second-moment bounds
 197 are valid when conditioning on $(\mathcal{F}_k, \Omega_T)$ for $k \leq T-1$).*

198 *Suppose $\mathbf{w}_1 \in \mathcal{N}_r$ and use a constant stepsize $\alpha_k = \bar{\alpha}$ such that*

$$0 < \bar{\alpha} \leq \frac{\mu}{\hat{L} K_G} \quad (\text{if } K_G > 0), \quad \text{and} \quad 0 < \bar{\alpha} < \frac{1}{\mu \hat{\mu}_{\text{PL}}}.$$

199 *Define*

$$\rho := \bar{\alpha} \hat{\mu}_{\text{PL}} \mu \in (0, 1), \quad C := \frac{\bar{\alpha} \hat{L} K}{2 \hat{\mu}_{\text{PL}} \mu}, \quad B := \frac{\alpha_{\text{QG}}}{2} r^2.$$

200 *For all $1 \leq k \leq T$,*

$$\mathbb{E}[F(\mathbf{w}_k) - F_* \mid \tau > T] \leq C + (1 - \rho)^{k-1} (F(\mathbf{w}_1) - F_* - C).$$

201 *The probability of remaining in \mathcal{N}_r up to time T satisfies*

$$\mathbb{P}(\tau > T) \geq \left[1 - \frac{F(\mathbf{w}_1) - F_* + \frac{\hat{L}}{2} \bar{\alpha}^2 K (T-1)}{B} - \sum_{k=1}^{T-1} \delta_k \right]_+,$$

202 *where $[x]_+ := \max\{0, x\}$.*

203 **Theorem 3.6** (Diminishing learning rate in a local basin up to a finite horizon). *Fix radii $0 < r < r_+$ and a
204 horizon $T \geq 1$, and let*

$$\tau := \inf\{k \geq 1 : \mathbf{w}_k \notin \mathcal{N}_r\}, \quad \Omega_T := \{\tau > T\}.$$

205 *Assume: (i) Assumptions 4 and 6 hold on \mathcal{N}_r ; (ii) Assumption 5 holds on a convex set \mathcal{V} with $\mathcal{N}_{r_+} \subset \mathcal{V} \subseteq \mathcal{U}$;
206 (iii) Assumption 7 holds on \mathcal{N}_{r_+} ; (iv) Assumption 8 holds with horizon T and failure probabilities $(\delta_k)_{k=1}^{T-1}$;
207 and (v) the conditional-moment version of Assumption 6 holds on Ω_T .*

208 *Suppose $\mathbf{w}_1 \in \mathcal{N}_r$ and use harmonic stepsizes*

$$\alpha_k = \frac{\beta}{\gamma + k}, \quad \gamma > 0,$$

209 *with*

$$0 < \alpha_1 = \frac{\beta}{\gamma + 1} \leq \frac{\mu}{\hat{L}K_G} \quad (\text{if } K_G > 0), \quad \text{and} \quad \beta > \frac{1}{\mu\hat{\mu}_{\text{PL}}} \quad (\text{equivalently } a := \beta\mu\hat{\mu}_{\text{PL}} > 1).$$

210 *Define*

$$m := \mu\hat{\mu}_{\text{PL}}, \quad c := \frac{\hat{L}K}{2}, \quad B := \frac{\alpha_{\text{QG}}}{2} r^2, \quad \nu := \max\left\{\frac{c\beta^2}{\beta m - 1}, (\gamma + 1)[F(\mathbf{w}_1) - F_*]\right\}.$$

211 *For all $1 \leq k \leq T$,*

$$\mathbb{E}[F(\mathbf{w}_k) - F_* | \tau > T] \leq \frac{\nu}{\gamma + k}.$$

212 *The probability of remaining in \mathcal{N}_r up to time T satisfies*

$$\mathbb{P}(\tau > T) \geq \left[1 - \frac{F(\mathbf{w}_1) - F_* + c \sum_{k=1}^{T-1} \alpha_k^2}{B} - \sum_{k=1}^{T-1} \delta_k\right]_+,$$

213 *where $[x]_+ := \max\{0, x\}$.*

214 *Theorem 3.5 (fixed stepsize) and Theorem 3.6 (harmonic stepsizes) characterize late-stage optimization *after*
215 the iterates have entered a well-behaved local basin \mathcal{N}_r . Both results are stated on the finite-horizon survival
216 event*

$$\Omega_T := \{\tau > T\}, \quad \tau := \inf\{k \geq 1 : \mathbf{w}_k \notin \mathcal{N}_r\},$$

217 *so that along Ω_T the local \mathbf{M} -smoothness and local \mathbf{M} -PL inequalities apply to the entire trajectory up
218 to time T and yield explicit descent recursions. With a constant stepsize $\bar{\alpha}$, Theorem 3.5 gives conditional
219 geometric contraction to the noise floor $C = \frac{\bar{\alpha}\hat{L}K}{2\hat{\mu}_{\text{PL}}\mu}$, whereas with harmonic stepsizes $\alpha_k = \beta/(\gamma + k)$,
220 Theorem 3.6 yields the conditional $\mathcal{O}(1/k)$ rate. In both cases, the constants are *local* and expressed in
221 the \mathbf{M} -geometry. Unlike global strongly convex analyses, no global curvature or global variance control is
222 required; the bounds depend only on the basin actually explored by the iterates.*

223 *The basin-stability guarantees are also local, and they make two distinct failure mechanisms explicit. The
224 first is an objective barrier controlled by the local QG constant α_{QG} and the basin radius r through*

$$B := \frac{\alpha_{\text{QG}}}{2} r^2,$$

225 *which quantifies the minimum objective increase needed to reach the boundary $\mathcal{N}_{r_+} \setminus \mathcal{N}_r$. The second is one-
226 step overshoot: Assumption 8 allows rare updates that jump from \mathcal{N}_r to outside the enlarged neighborhood
227 \mathcal{N}_{r_+} , with conditional failure probabilities δ_k . Here, $\sum_{k=1}^{T-1} \delta_k$ quantifies the accumulated overshoot risk: if
228 the tails/second moments are large, or if the basin margin $\Delta = r_+ - r$ is small, then δ_k may be large, and
229 the stability bound becomes conservative.*

230 *Because all constants in the local bounds are \mathbf{M} -dependent, a well-chosen preconditioner \mathbf{M} can improve late-
231 stage behavior by: (i) enhancing local conditioning (increasing $\hat{\mu}_{\text{PL}}$ and/or decreasing \hat{L} , thereby strengthening
232 contraction); (ii) reducing the preconditioned noise level K ; and (iii) improving stability by reducing the
233 overshoot probabilities δ_k (e.g., via smaller $\mathbb{E}[\|g_k\|_{\mathbf{M}^{-1}}^2]$ and/or a larger margin $\Delta = r_+ - r$) and, when
234 aligned with normal-space curvature, by increasing the barrier parameter $B = \frac{\alpha_{\text{QG}}}{2} r^2$.*

235 **3.3 Practical preconditioners for SGD**

236 A wide range of preconditioning strategies are used in modern machine learning. On the first-order side,
 237 adaptive methods such as Adam (Kingma & Ba, 2017), AMSGrad (Reddi et al., 2018), PAdam (Chen
 238 et al., 2020), and Yogi (Zaheer et al., 2018) implicitly apply *diagonal* preconditioners by rescaling gradients
 239 with running estimates of coordinatewise second moments. On the second-order side, *curvature-aware*
 240 preconditioners exploit Hessian or Fisher Information Matrix (FIM) structure, including the empirical
 241 FIM (Schraudolph, 2002), full or mini-batch Hessians (Fletcher, 2013; Garg et al., 2024), mini-batch
 242 quasi-Newton updates (Griffin et al., 2022), and Kronecker-factored FIM (K-FAC) (Martens & Grosse, 2015).
 243 Classical schemes such as L-BFGS (Liu & Nocedal, 1989; Chen et al., 2014) can also be viewed as low-rank,
 244 history-based preconditioners. Appendix B.2 summarizes these approaches and their computational trade-offs.
 245 The convergence analysis in Sections 3.1–3.2 suggests two practical mechanisms through which preconditioners
 246 shape late-stage behavior:

247

- 248 • *Local conditioning.* Curvature-aware preconditioners (e.g., Fisher, Gauss–Newton, Hessian, K-FAC)
 249 tend to reduce the metric–smoothness constant \hat{L} and can increase the local PL constant $\hat{\mu}_{\text{PL}}$. In our
 250 bounds, this improves the effective local condition number $\hat{L}/\hat{\mu}_{\text{PL}}$, permits larger admissible fixed
 learning rates $\alpha \leq \mu/(\hat{L}K_G)$, and reduces the leading constant under diminishing learning rates.

251

- 252 • *Noise attenuation.* Preconditioners aligned with the gradient-noise structure reduce the preconditioned
 253 noise level K in the late-stage regime. Together with improved conditioning (smaller \hat{L}/\hat{c} or $\hat{L}/\hat{\mu}_{\text{PL}}$),
 254 this lowers the noise floor, which scales with their *product*. Fisher-based and related methods are
 especially effective because they explicitly incorporate gradient statistics.

255 These two mechanisms—improved conditioning and reduced preconditioned noise—match the behavior
 256 observed in Section 4. Curvature-matched preconditioners (Fisher, Gauss–Newton, K-FAC, Hessian) typically
 257 yield faster late-stage contraction by reducing \hat{L} and, in some cases, increasing $\hat{\mu}_{\text{PL}}$, while their use of gradient
 258 second-moment information tends to reduce K . Adaptive/diagonal methods likewise lower K by damping
 259 high-variance coordinates, though their alignment with curvature is typically weaker. [Recent theory further
 260 suggests that in anisotropic settings, Kronecker-structured preconditioning can be statistically necessary for
 261 efficient feature learning, whereas entry-wise/diagonal scaling offers only partial improvements](#) (Zhang et al.,
 262 2025).

263 **4 Numerical results**

264 Many machine-learning benchmarks illustrate the benefits of preconditioned SGD (e.g., Schmidt et al. (2021);
 265 Schneider et al. (2019)), but our emphasis is on SciML, where driving the loss to very small values is tightly
 266 linked to physical fidelity, numerical stability, and constraint satisfaction (Kaplan et al., 2020; Swersky et al.,
 267 2011). We therefore structure the experiments in two parts.

268 First, we analyze a *diagnostic quadratic model* in which all the quantities in our theory— \hat{L} , $\hat{\mu}_{\text{PL}}$, and the
 269 preconditioned noise level K —admit closed forms. This allows us to directly compute the geometry– and
 270 noise–dependent metrics from Sections 3.1–3.2 and verify their influence on rate and floor.

271 Second, we examine three representative SciML problems: noisy Franke surface regression (Franke, 1979), a
 272 Poisson–type PINN, and Green’s–function learning for diffusion and convection–diffusion (Zhang et al., 2024;
 273 Rathore et al., 2024; Hao et al., 2024; Xu et al., 2025), to see how the theoretical mechanisms are reflected in
 274 practical settings.

275 **4.1 Diagnostic quadratic model**

276 To isolate the effects predicted by the theory, we consider the quadratic objective

$$F(\mathbf{w}) = \frac{1}{2}(\mathbf{w} - \mathbf{w}^*)^\top \mathbf{H}(\mathbf{w} - \mathbf{w}^*) + F_*, \quad \mathbf{H} \succeq 0,$$

here \mathbf{H} specifies curvature. We test two simple, analytically tractable choices: Euclidean SGD ($\mathbf{M} = \mathbf{I}$) and a low-rank curvature-aware preconditioner $\mathbf{M} = \mathbf{I} + \mathbf{U}_s(\tilde{\mathbf{\Lambda}}_s - \mathbf{I})\mathbf{U}_s^\top$, where \mathbf{U}_s contains the top (or bottom) s eigenvectors of \mathbf{H} and $\tilde{\mathbf{\Lambda}}_s$ is a diagonal matrix. This model captures the essential effect of curvature information. We used a fixed learning rate.

Instead of forming a dataset, we synthesize unbiased mini-batch gradients

$$g_k = \nabla F(\mathbf{w}_k) + \zeta_k, \quad \mathbb{E}[\zeta_k] = 0, \quad \text{Cov}(\zeta_k) = \frac{1}{B}\mathbf{\Sigma}.$$

To match the second-order statistics of least-squares problems near \mathbf{w}^* , we set $\mathbf{\Sigma} = \sigma^2\mathbf{H}$, giving $K = \frac{\sigma^2}{B}\text{tr}(\mathbf{M}^{-1}\mathbf{H})$. We choose $d = 100$ and construct $\mathbf{H} = \mathbf{U}\mathbf{\Lambda}\mathbf{U}^\top$ with $\mathbf{\Lambda}$ log-uniform grid on $[10^{-2}, 10^2]$ and \mathbf{U} Haar-distributed. We set $\mathbf{w}^* = 0$, $F_* = 0$, and initialize $\mathbf{w}_1 \sim \mathcal{N}(0, 10^{-4}\mathbf{I})$, and report averages over 30 runs. To illustrate how individual eigenvalues affect constants $(\hat{L}, \hat{\mu}_{PL}, K)$, we design three groups of tests targeting different part of the spectrum of \mathbf{H} .

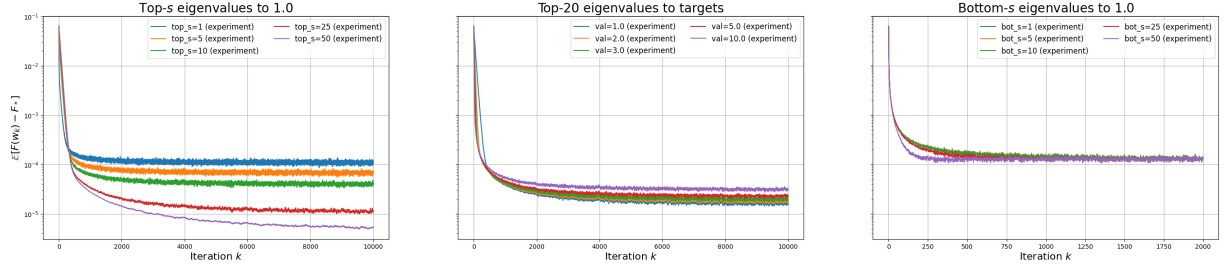


Figure 1: Convergence behavior under different deflation-based preconditioners. Left: deflating the largest s eigenvalues ($s \in \{1, 5, 10, 25, 50\}$). Middle: deflating the top 20 eigenvalues to target values $1.0, 2.0, 3.0, 5.0, 10.0$. Right: deflating the smallest s eigenvalues ($s \in \{1, 5, 10, 25, 50\}$).

Figure 1 shows how deflating different parts of the spectrum of \mathbf{H} affects the key theoretical constants. Denote the eigenpairs of \mathbf{H} as $(\lambda_i, \mathbf{u}_i)$, and let \mathbf{U}_s contain the selected eigenvectors. We construct a spectral preconditioner of the form $\mathbf{M} = \mathbf{I} + \mathbf{U}_s(\tilde{\mathbf{\Lambda}}_s - \mathbf{I})\mathbf{U}_s^\top$, where $\tilde{\mathbf{\Lambda}}_s = \text{diag}(\tau_1, \dots, \tau_s)$ assigns a target value τ_i to the i -th chosen eigendirection. Deflating the largest s eigenvalues (left panel)—i.e., setting $\tau_i = \lambda_i$ so that these preconditioned eigenvalues become 1—reduces the smoothness constant \hat{L} and the noise level $K = \frac{\sigma^2}{B}\text{tr}(\mathbf{M}^{-1}\mathbf{H})$ while leaving $\hat{\mu}_{PL}$ unchanged, yielding a lower noise floor.

To isolate the effect of the noise term, the middle panel fixes $\hat{\mu}_{PL}$. It deflates the top 20 eigenvalues into a common value v lying between λ_{21} and λ_d by setting $\tau_i = \lambda_i/v$, so that \hat{L} and $\hat{\mu}_{PL}$ remain unchanged while K varies. The resulting steady-state losses track this change in K , in line with the predicted noise-floor scaling. Deflating the smallest s eigenvalues (right panel)—that is, selecting the bottom eigenvectors and assigning target values τ_i equal to these smallest eigenvalues so that the preconditioned eigenvalues λ_i/τ_i move to 1—does increase $\hat{\mu}_{PL}$, but it simultaneously enlarges K . The two effects counterbalance each other, yielding only modest overall gains, consistent with the predicted noise-floor behavior.

4.2 SciML problems

We then briefly summarize the three SciML tasks used to evaluate late-stage optimization behavior under different preconditioners.

Noisy Franke surface regression. The Franke function is a classical multiscale benchmark consisting of several Gaussian peaks with heterogeneous length scales. We sample 256 points uniformly in $[0, 1]^2$ and corrupt the values with Gaussian noise $\varepsilon \sim \mathcal{N}(0, 10^{-4})$. The combination of multiscale structure and observational noise yields a loss landscape with varying curvature, making it well suited for evaluating how preconditioning affects convergence in practice. The target surface is

$$f(x, y) = 0.75e^{-\frac{(9x-2)^2+(9y-2)^2}{4}} + 0.75e^{-\frac{(9x+1)^2}{49}-\frac{9y+1}{10}} + 0.5e^{-\frac{(9x-7)^2+(9y-3)^2}{4}} - 0.2e^{-(9x-4)^2-(9y-7)^2}.$$

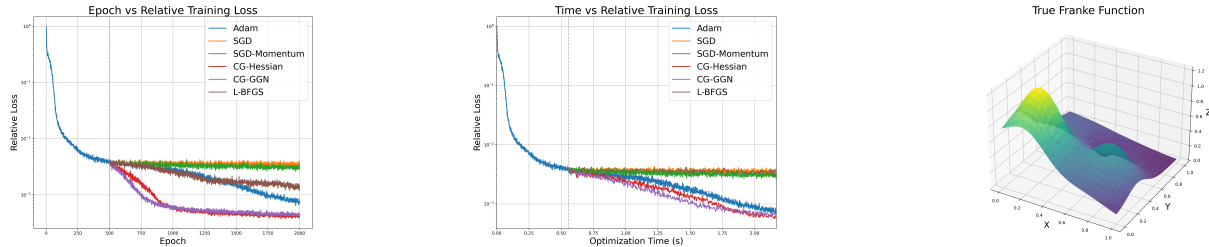


Figure 2: Franke-function regression (mean over 5 runs). Left: training loss vs. epochs with the switch to Phase II at epoch 500. Center: training loss vs. wall-clock time. Right: Franke surface.

308 **Physics-informed neural networks (PINNs).** We train a PINN to solve the 2D Poisson problem

$$-\Delta u = f(x, y) = 8\pi^2 \sin(2\pi x) \sin(2\pi y) \quad \text{in } (0, 1)^2, \quad u = 0 \text{ on } \partial[0, 1]^2,$$

309 whose exact solution is $u(x, y) = \sin(2\pi x) \sin(2\pi y)$. The training set includes 1,000 interior residual points
 310 and 200 boundary points. The weighted loss (PDE residual weight 1.0, boundary weight 100.0) produces a
 311 challenging composite landscape known to stress first-order methods (Krishnapriyan et al., 2021). The right
 312 panel of Fig. 3 visualizes the source term $f(x, y)$.

313 **Green's-function learning.** We learn Green's functions for the 1D convection-diffusion operator

$$\mathcal{L}u := -\nu u'' + \beta u', \quad u(0) = u(1) = 0,$$

314 under two regimes: (i) diffusion-dominated ($\nu = 1.0, \beta = 0$) and (ii) convection-dominated ($\nu = 0.1, \beta = 1.0$).
 315 The Green's function satisfies $\mathcal{L}G(x, y) = \delta(x - y)$, where we approximate the delta distribution by a narrow
 316 Gaussian with width $\sigma = 0.01$. Training uses: (a) 1,000 uniformly sampled (x, y) pairs for PDE residuals, (b)
 317 500 near-diagonal samples ($|x - y|$ small) to capture the near-singularity, and (c) 200 boundary samples. This
 318 produces a highly multiscale and stiffness-dominated optimization problem, ideal for testing curvature-aware
 319 preconditioners.

320 **Baselines and protocol.** Across all SciML tasks, we compare vanilla SGD, momentum, Adam, L-BFGS,
 321 and curvature-aware preconditioners (CG-Hessian and CG-GGN/Fisher). Matrix-free CG with a fixed
 322 iteration budget is used to apply Hessian or Gauss-Newton/Fisher updates. Following standard SciML
 323 practice, we adopt a two-phase schedule: Phase I uses Adam to reach a comparable basin; Phase II switches
 324 to the target optimizer to isolate late-stage behavior. We report loss vs. epochs and wall-clock time, with all
 325 architectural and implementation details in Appendix D. All implementations use JAX (Bradbury et al.,
 326 2018); code and data are available in the supplemental material.

327 4.3 Noisy data regression

328 After the Adam warm start (Phase I), Phase II separates the methods (Fig. 2): *Adam*, *L-BFGS*, *CG-*
 329 *GGN*, and *CG-Hessian* descend faster than *SGD* and *SGD+Momentum*. The two curvature-aware variants,
 330 *CG-Hessian* and *CG-GGN*, track one another closely—showing similar contraction and reaching essentially
 331 the same loss floor. The similar performance of *CG-Hessian* and *CG-GGN* suggests that both methods
 332 provide comparable normal-space curvature and covariance matrix structure approximation. Adam's diagonal
 333 rescaling and *L-BFGS*'s low-rank curvature information also mitigate anisotropy and stabilize noisy directions,
 334 which explains their advantage over *SGD*. In wall-clock time, the faster descent of curvature-aware methods
 335 compensates for their higher per-step cost.

336 4.4 Physics-informed neural networks (PINNs)

337 With the same two-phase protocol, Phase II shows a consistent ranking (Fig. 3). At the bottom, *Adam*
 338 and *SGD/SGD+Momentum* lack explicit curvature information and progress slowly. *L-BFGS* achieves

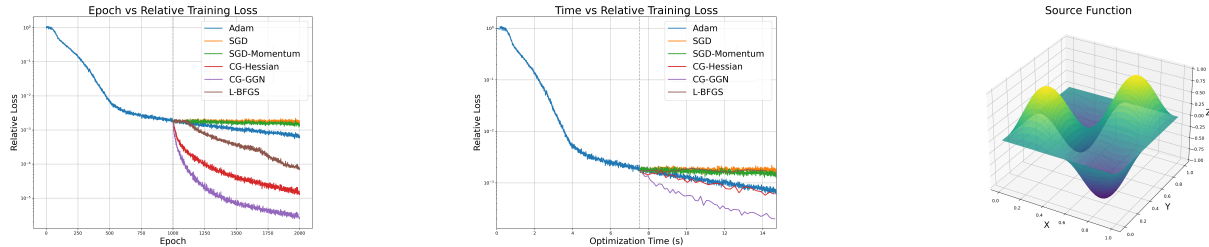


Figure 3: PINN for a Poisson-type PDE (mean over 5 runs). Left: training loss vs. epochs with Phase I → Phase II at epoch 1,000. Center: training loss vs. wall-clock time. Right: source term.

339 intermediate performance: it captures limited curvature through its low-rank approximation and line search,
 340 but the memory constraint prevents it from matching the full curvature captured by the two *CG* methods.
 341 At the top tier, *CG-GGN* and *CG-Hessian* both achieve better performance as curvature-aware methods,
 342 with *CG-GGN* showing a slight advantage.
 343 For PINNs, which minimize weighted least-squares residuals, the Gauss–Newton approximation $\mathbf{J}^\top \mathbf{J}$ is
 344 naturally aligned with the gradient covariance structure and thus provides more effective noise attenua-
 345 tion—consistent with our theory, where the preconditioned noise level is governed by $\text{tr}(\mathbf{M}^{-1} \boldsymbol{\Sigma}(\mathbf{w}))$ in the late
 346 stage. The Hessian approximation, by contrast, can introduce negative curvature and additional anisotropy.
 347 In wall-clock time, *CG-GGN* achieves the best accuracy within a comparable time budget, despite its higher
 348 per-step cost.

349 4.5 Green's function learning

350 After Phase I, Phase II again shows a clear separation of methods (Figs. 4–5). In both the diffusion- and
 351 convection-dominated cases, *CG-GGN* continues to drive the loss down, whereas *CG-Hessian*, *L-BFGS*,
 352 *Adam*, *SGD*, and *SGD+Momentum* quickly form a tight cluster and improve only marginally. Compared with
 353 the earlier PINNs experiment, the Green's–function tasks are more near-singular due to the smoothed-delta
 354 forcing, leading to a more challenging, highly anisotropic optimization problem.

355 Although we did not directly measure the local constants $(\hat{L}, \hat{\mu}_{PL}, K)$ on this run, the observed advantage
 356 of *CG-GGN* is consistent with the structure of PINN objectives. First, for squared-residual losses, the
 357 Gauss–Newton/Fisher matrix is positive semidefinite, avoiding the negative-curvature directions introduced
 358 by second-derivative terms in the exact Hessian. This makes the preconditioner more stable and better
 359 suited to CG. Second, Fisher-type preconditioners are built from gradient second moments and therefore tend
 360 to *whiten* gradient noise, reducing the preconditioned noise level K . In contrast, a Hessian preconditioner
 361 includes second-order terms that are often misaligned with the gradient-noise covariance, and the damping
 362 needed to handle indefiniteness diminishes curvature gains while weakening noise attenuation.

363 These two effects—better alignment with useful curvature and more effective noise whitening—explain why
 364 *CG-GGN* reaches lower losses within comparable wall-clock time, despite its higher per-step cost.

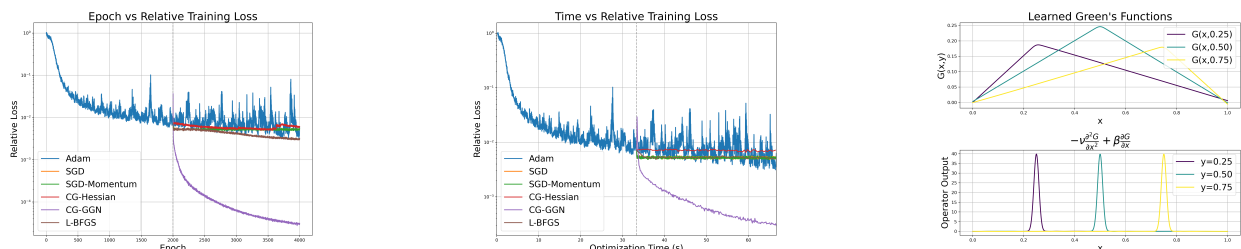


Figure 4: Laplacian Green's function learning (mean over 5 runs). Left: loss vs. epochs with Phase I → Phase II at epoch 2,000. Center: loss vs. wall-clock time. Right: learned $G(x, y)$ for three source locations and operator checks.

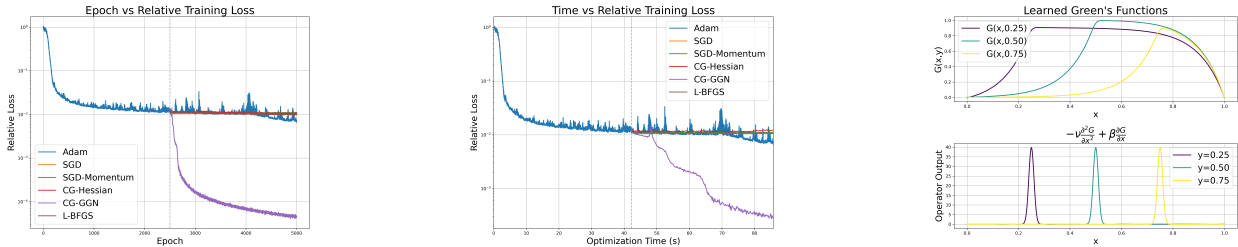


Figure 5: Convection-diffusion Green's function learning (mean over 5 runs). Left: loss vs. epochs with Phase I → Phase II at epoch 2,500. Center: loss vs. wall-clock time. Right: learned $G(x, y)$ for three source locations and operator checks.

365 The right panels of Figs. 4 and 5 display the learned Green's functions $G(x, y)$ at three representative source locations y together with simple operator and boundary checks for CG-GGN. The kernels are localized 366 around the source locations and decay toward the Dirichlet boundaries, and the corresponding operator 367 evaluations produce narrow spikes at $x = y$, in line with the smoothed-delta forcing used in the training 368 loss. This suggests that the lower training losses achieved by CG-GGN reflect a reasonable Green's-function 369 approximation rather than a purely numerical artifact.

370 We conclude the numerical experiments by connecting the CG-GGN preconditioner to the theoretical 371 convergence framework developed in this paper. We empirically examine the quantities L and K that govern 372 the convergence of preconditioned SGD for the PINNs problem and two Green's function learning problems. 373 Because a CG-based preconditioner with only a few iterations typically does not significantly alter the 374 cluster of near-zero eigenvalues, we treat the M -PL constant as unchanged and attribute the quality of the 375 preconditioner primarily to its effect on L and K . For these three problems, we fix the random seed to 42 376 and analyze the network parameters at epoch 250 in Phase II. After preconditioning, the L value reduced by 377 factors of 78x, 3710x, and 1923x, respectively. We additionally quantify the impact of preconditioning on the 378 noise level K . Using the same network parameters w , we sample 100 independent mini-batches, construct the 379 preconditioner M^{-1} from the first batch, and observe that after preconditioning the estimated trace of the 380 gradient-noise covariance matrix is reduced by factors of 12x, 1505x, and 203x, respectively. This substantial 381 reduction demonstrates that the CG-GGN preconditioner effectively attenuates gradient noise. Consistent 382 with our theory, the combined improvements in conditioning and noise reduction yield both faster linear 383 convergence and a significantly lower asymptotic noise floor.

385 5 Conclusion

386 We developed a local, geometry-aware theory for preconditioned SGD that makes two effects explicit: (1) the 387 rate inside a basin is controlled by a preconditioner-dependent condition number in the M -metric, and (2) 388 the noise floor is governed by the preconditioned noise. We additionally obtained a basin-stability guarantee, 389 giving an explicit probability that iterates remain in a region where these local properties hold. Together, 390 the results motivate a simple rule: choose M to improve local conditioning while suppressing noise in the 391 M^{-1} -norm.

392 A key next direction is *covariance-aware* preconditioning. Our bounds suggest that effective design should 393 jointly target conditioning and noise attenuation, motivating structured covariance models and adaptive 394 schemes that update curvature and noise statistics simultaneously. Extending basin-stability guarantees 395 to nonstationary noise and developing online diagnostics for the local constants would move toward fully 396 adaptive, geometry- and noise-aware SGD.

397 **References**

398 Shunichi Amari. A theory of adaptive pattern classifiers. *IEEE Transactions on Electronic Computers*, EC-16
 399 (3):299–307, 1967. ISSN 0367-7508. doi: 10.1109/PGEC.1967.264666. URL <https://ieeexplore.ieee.org/document/4039068>. Conference Name: IEEE Transactions on Electronic Computers.

401 Amit Attia and Tomer Koren. Sgd with adagrad stepsizes: Full adaptivity with high probability to unknown
 402 parameters, unbounded gradients and affine variance. In *International Conference on Machine Learning*,
 403 pp. 1147–1171. PMLR, 2023.

404 David GT Barrett and Benoit Dherin. Implicit gradient regularization. *arXiv preprint arXiv:2009.11162*,
 405 2020.

406 Albert S. Berahas, Jorge Nocedal, and Martin Takáč. A multi-batch l-bfgs method for machine learning,
 407 2016. URL <https://arxiv.org/abs/1605.06049>.

408 Julius R. Blum. Approximation methods which converge with probability one. *The Annals of Mathematical
 409 Statistics*, 25(2):382–386, 1954. ISSN 0003-4851, 2168-8990. doi: 10.1214/aoms/1177728794. URL
 410 [https://projecteuclid.org/journals/annals-of-mathematical-statistics/volume-25/issue-2/](https://projecteuclid.org/journals/annals-of-mathematical-statistics/volume-25/issue-2/Approximation-Methods-which-Converge-with-Probability-one/10.1214/aoms/1177728794.full)
 411 [Approximation-Methods-which-Converge-with-Probability-one/10.1214/aoms/1177728794.full](https://projecteuclid.org/journals/annals-of-mathematical-statistics/volume-25/issue-2/Approximation-Methods-which-Converge-with-Probability-one/10.1214/aoms/1177728794.full).
 412 Publisher: Institute of Mathematical Statistics.

413 Raghu Bollapragada, Dheevatsa Mudigere, Jorge Nocedal, Hao-Jun Michael Shi, and Ping Tak Peter Tang. A
 414 progressive batching l-bfgs method for machine learning, 2018. URL <https://arxiv.org/abs/1802.05374>.

415 Léon Bottou, Frank E. Curtis, and Jorge Nocedal. Optimization methods for large-scale machine learn-
 416 ing. *SIAM Review*, 60(2):223–311, 2018. doi: 10.1137/16M1080173. URL <https://doi.org/10.1137/16M1080173>.

418 James Bradbury, Roy Frostig, Peter Hawkins, Matthew James Johnson, Chris Leary, Dougal Maclaurin,
 419 George Necula, Adam Paszke, Jake VanderPlas, Skye Wanderman-Milne, and Qiao Zhang. JAX: composable
 420 transformations of Python+NumPy programs, 2018. URL <http://github.com/jax-ml/jax>.

421 Han Chan. Some methods of unconstrained minimization. *USSR Computational Mathematics and Mathe-
 422 matical Physics*, 19(2):31–44, 1979. ISSN 0041-5553. doi: [https://doi.org/10.1016/0041-5553\(79\)90004-1](https://doi.org/10.1016/0041-5553(79)90004-1).
 423 URL <https://www.sciencedirect.com/science/article/pii/0041555379900041>.

424 Jinghui Chen, Dongruo Zhou, Yiqi Tang, Ziyan Yang, Yuan Cao, and Quanquan Gu. Closing the generalization
 425 gap of adaptive gradient methods in training deep neural networks. In Christian Bessiere (ed.), *Proceedings
 426 of the Twenty-Ninth International Joint Conference on Artificial Intelligence, IJCAI-20*, pp. 3267–3275.
 427 International Joint Conferences on Artificial Intelligence Organization, 7 2020. doi: 10.24963/ijcai.2020/452.
 428 URL <https://doi.org/10.24963/ijcai.2020/452>. Main track.

429 Weizhu Chen, Zhenghao Wang, and Jingren Zhou. Large-scale l-bfgs using mapreduce. In *Proceedings of
 430 the 28th International Conference on Neural Information Processing Systems - Volume 1*, NIPS’14, pp.
 431 1332–1340, Cambridge, MA, USA, 2014. MIT Press.

432 John Duchi, Elad Hazan, and Yoram Singer. Adaptive subgradient methods for online learning and stochastic
 433 optimization. *Journal of Machine Learning Research*, 12:2121–2159, 2011.

434 Matthew Faw, Isidoros Tziotis, Constantine Caramanis, Aryan Mokhtari, Sanjay Shakkottai, and Rachel
 435 Ward. The power of adaptivity in sgd: Self-tuning step sizes with unbounded gradients and affine variance.
 436 In *Conference on Learning Theory*, pp. 313–355. PMLR, 2022.

437 R. Fletcher. *Practical Methods of Optimization*. Wiley, 2013. ISBN 978-1-118-72318-0. URL https://books.google.com/books?id=_WuAvIx0EE4C.

439 Francis Bach. *Learning Theory from First Principles*. Adaptive computation and machine learning series.
 440 MIT Press, 2 edition, 2024. ISBN 978-0-262-04944-3.

441 Richard Franke. A Critical Comparison of Some Methods for Interpolation of Scattered Data. Technical
442 report, Graduate School of Operational and Information Sciences (GSOIS), 1979. URL <https://apps.dtic.mil/sti/citations/ADA081688>.

444 Sachin Garg, Albert S. Berahas, and Michał Dereziński. Second-order information promotes mini-batch
445 robustness in variance-reduced gradients, 2024. URL <https://arxiv.org/abs/2404.14758>.

446 Guillaume Garrigos and Robert M. Gower. Handbook of convergence theorems for (stochastic) gradient
447 methods, 2024. URL <http://arxiv.org/abs/2301.11235>.

448 Behrooz Ghorbani, Shankar Krishnan, and Ying Xiao. An investigation into neural net optimization via
449 hessian eigenvalue density. In Kamalika Chaudhuri and Ruslan Salakhutdinov (eds.), *Proceedings of the 36th*
450 *International Conference on Machine Learning*, volume 97 of *Proceedings of Machine Learning Research*, pp.
451 2232–2241. PMLR, 09–15 Jun 2019. URL <https://proceedings.mlr.press/v97/ghorbani19b.html>.

452 Joshua D Griffin, Majid Jahani, Martin Takáč, Seyedalireza Yektamaram, and Wenwen Zhou. A minibatch
453 stochastic Quasi-Newton method adapted for nonconvex deep learning problems. *Optimization Online*,
454 2022.

455 Vineet Gupta, Tomer Koren, and Yoram Singer. Shampoo: Preconditioned stochastic tensor optimization.
456 In Jennifer Dy and Andreas Krause (eds.), *Proceedings of the 35th International Conference on Machine*
457 *Learning*, volume 80 of *Proceedings of Machine Learning Research*, pp. 1842–1850. PMLR, 10–15 Jul 2018.
458 URL <https://proceedings.mlr.press/v80/gupta18a.html>.

459 Wenrui Hao, Rui Peng Li, Yuanzhe Xi, Tianshi Xu, and Yahong Yang. Multiscale neural networks for
460 approximating green’s functions, 2024. URL <https://arxiv.org/abs/2410.18439>.

461 Geoffrey Hinton. Neural networks for machine learning lecture 6e: rmsprop: Divide the gradient by a running
462 average of its recent magnitude, 2014. URL https://www.cs.toronto.edu/~tijmen/csc321/slides/lecture_slides_lec6.pdf.

464 Shun ichi Amari, Jimmy Ba, Roger Baker Grosse, Xuechen Li, Atsushi Nitanda, Taiji Suzuki, Denny Wu, and
465 Ji Xu. When does preconditioning help or hurt generalization? In *International Conference on Learning*
466 *Representations*, 2021. URL https://openreview.net/forum?id=S724o4_WB3.

467 Satoshi Ishikawa and Ryo Karakida. On the parameterization of second-order optimization effective towards
468 the infinite width. In *The Twelfth International Conference on Learning Representations*, 2024. URL
469 <https://openreview.net/forum?id=g8sGBSQjYk>.

470 Jared Kaplan, Sam McCandlish, Tom Henighan, Tom B. Brown, Benjamin Chess, Rewon Child, Scott
471 Gray, Alec Radford, Jeffrey Wu, and Dario Amodei. Scaling laws for neural language models, 2020. URL
472 <https://arxiv.org/abs/2001.08361>.

473 Hamed Karimi, Julie Nutini, and Mark Schmidt. Linear convergence of gradient and proximal-gradient
474 methods under the polyak-łojasiewicz condition. In Paolo Frasconi, Niels Landwehr, Giuseppe Mancuso, and
475 Jilles Vreeken (eds.), *Machine Learning and Knowledge Discovery in Databases*, pp. 795–811, Cham, 2016.
476 Springer International Publishing. ISBN 978-3-319-46128-1.

477 Ahmed Khaled and Peter Richtárik. Better theory for SGD in the nonconvex world. *Transactions on Machine*
478 *Learning Research*, 2023. ISSN 2835-8856. URL <https://openreview.net/forum?id=AU4qHN2Vks>. Survey
479 Certification.

480 Diederik P. Kingma and Jimmy Ba. Adam: A method for stochastic optimization, 2017. URL <http://arxiv.org/abs/1412.6980>.

482 Tomer Koren, Roi Livni, Yishay Mansour, and Uri Sherman. Benign underfitting of stochastic gradient
483 descent. *Advances in Neural Information Processing Systems*, 35:19605–19617, 2022.

484 Aditi Krishnapriyan, Amir Gholami, Shandian Zhe, Robert Kirby, and Michael W Mahoney. Characterizing
 485 possible failure modes in physics-informed neural networks. In M. Ranzato, A. Beygelzimer, Y. Dauphin,
 486 P.S. Liang, and J. Wortman Vaughan (eds.), *Advances in Neural Information Processing Systems*, volume 34,
 487 pp. 26548–26560. Curran Associates, Inc., 2021. URL https://proceedings.neurips.cc/paper_files/paper/2021/file/df438e5206f31600e6ae4af72f2725f1-Paper.pdf.

488

489 Frederik Kunstner, Lukas Balles, and Philipp Hennig. Limitations of the empirical fisher approximation
 490 for natural gradient descent. In *Proceedings of the 33rd International Conference on Neural Information
 491 Processing Systems*, Red Hook, NY, USA, 2019. Curran Associates Inc.

492 Susanna Lange, Kyle Helfrich, and Qiang Ye. Batch normalization preconditioning for neural network training.
 493 *Journal of Machine Learning Research*, 23(72):1–41, 2022.

494 Xi-Lin Li. Preconditioned stochastic gradient descent. *IEEE Transactions on Neural Networks and Learning
 495 Systems*, 29(5):1454–1466, 2018. doi: 10.1109/TNNLS.2017.2672978.

496 Dong C. Liu and Jorge Nocedal. On the limited memory BFGS method for large scale optimization.
 497 *Mathematical Programming*, 45(1):503–528, August 1989. ISSN 1436-4646. doi: 10.1007/BF01589116. URL
 498 <https://doi.org/10.1007/BF01589116>.

499 Hong Liu, Zhiyuan Li, David Leo Wright Hall, Percy Liang, and Tengyu Ma. Sophia: A scalable stochastic
 500 second-order optimizer for language model pre-training. In *The Twelfth International Conference on
 501 Learning Representations*, 2024. URL <https://openreview.net/forum?id=3xHDeA8Noi>.

502 Ilya Loshchilov and Frank Hutter. Decoupled weight decay regularization. *arXiv preprint arXiv:1711.05101*,
 503 2017.

504 James Martens. New insights and perspectives on the natural gradient method. *Journal of Machine Learning
 505 Research*, 21(146):1–76, 2020. URL <http://jmlr.org/papers/v21/17-678.html>.

506 James Martens and Roger Grosse. Optimizing neural networks with kronecker-factored approximate curvature.
 507 In *Proceedings of the 32nd International Conference on International Conference on Machine Learning -
 508 Volume 37*, ICML’15, pp. 2408–2417. JMLR.org, 2015.

509 Pratik Rathore, Weimu Lei, Zachary Frangella, Lu Lu, and Madeleine Udell. Challenges in training pinns:
 510 a loss landscape perspective. In *Proceedings of the 41st International Conference on Machine Learning*,
 511 ICML’24. JMLR.org, 2024.

512 Sashank J. Reddi, Satyen Kale, and Sanjiv Kumar. On the convergence of adam and beyond. In *International
 513 Conference on Learning Representations*, 2018. URL <https://openreview.net/forum?id=ryQu7f-RZ>.

514 Herbert Robbins and Sutton Monro. A stochastic approximation method. *The Annals of Math-
 515 ematical Statistics*, 22(3):400–407, 1951. ISSN 0003-4851, 2168-8990. doi: 10.1214/aoms/1177729586. URL
 516 <https://projecteuclid.org/journals/annals-of-mathematical-statistics/volume-22/issue-3/A-Stochastic-Approximation-Method/10.1214/aoms/1177729586.full>. Publisher:
 517 Institute of Mathematical Statistics.

518

519 Levent Sagun, Utku Evci, V. Ugur Guney, Yann Dauphin, and Leon Bottou. Empirical analysis of the hessian
 520 of over-parametrized neural networks, 2018. URL <https://openreview.net/forum?id=rJrTwxbCb>.

521 Robin M Schmidt, Frank Schneider, and Philipp Hennig. Descending through a crowded valley - benchmarking
 522 deep learning optimizers. In Marina Meila and Tong Zhang (eds.), *Proceedings of the 38th International
 523 Conference on Machine Learning*, volume 139 of *Proceedings of Machine Learning Research*, pp. 9367–9376.
 524 PMLR, 18–24 Jul 2021. URL <https://proceedings.mlr.press/v139/schmidt21a.html>.

525 Frank Schneider, Lukas Balles, and Philipp Hennig. DeepOBS: A deep learning optimizer benchmark suite.
 526 In *International Conference on Learning Representations*, 2019. URL <https://openreview.net/forum?id=rJg6ssC5Y7>.

527

528 Nicol N. Schraudolph. Fast curvature matrix-vector products for second-order gradient descent. *Neural*
529 *Computation*, 14(7):1723–1738, 2002. ISSN 0899-7667, 1530-888X. doi: 10.1162/08997660260028683. URL
530 <https://direct.mit.edu/neco/article/14/7/1723-1738/6626>.

531 Kevin Swersky, Marc’Aurelio Ranzato, David Buchman, Benjamin Marlin, and Nando Freitas. On autoencoders
532 and score matching for energy based models. In Lise Getoor and Tobias Scheffer (eds.), *Proceedings of the*
533 *28th International Conference on Machine Learning (ICML-11)*, ICML ’11, pp. 1201–1208, New York, NY,
534 USA, June 2011. ACM. ISBN 978-1-4503-0619-5. URL <http://mldiscuss.appspot.com/venue/ICML/2011/article/622/>.

536 Tianshi Xu, Rui Peng Li, and Yuanzhe Xi. Neural approximate inverse preconditioners, 2025. URL
537 <https://arxiv.org/abs/2510.13034>.

538 Qiang Ye. Preconditioning for accelerated gradient descent optimization and regularization, 2024. URL
539 <https://arxiv.org/abs/2410.00232>.

540 Manzil Zaheer, Sashank Reddi, Devendra Sachan, Satyen Kale, and Sanjiv Kumar. Adaptive meth-
541 ods for nonconvex optimization. In S. Bengio, H. Wallach, H. Larochelle, K. Grauman, N. Cesa-
542 Bianchi, and R. Garnett (eds.), *Advances in Neural Information Processing Systems*, volume 31. Cur-
543 ran Associates, Inc., 2018. URL https://proceedings.neurips.cc/paper_files/paper/2018/file/90365351ccc7437a1309dc64e4db32a3-Paper.pdf.

545 Handi Zhang, Langchen Liu, and Lu Lu. Federated scientific machine learning for approximating functions and
546 solving differential equations with data heterogeneity, 2024. URL <https://arxiv.org/abs/2410.13141>.

547 Thomas TCK Zhang, Behrad Moniri, Ansh Nagwekar, Faraz Rahman, Anton Xue, Hamed Hassani, and
548 Nikolai Matni. On the concurrence of layer-wise preconditioning methods and provable feature learning.
549 In *Forty-second International Conference on Machine Learning*, 2025. URL <https://openreview.net/forum?id=aRUUFFycNh>.

551 Appendix

552 A Notation used in paper

553 In general, capital bold letters are matrices (\mathbf{A}), lower case bold letters are vectors (\mathbf{v}), and lower case Greek
 554 or Latin letters are constants (ν, c). Moreover, there are some notation that is used consistently throughout
 555 the paper. A reference table for these symbols is given in Table 1.

Table 1: Reference for recurring notation in the paper.

Symbol	Definition
k	iteration counter
\mathbf{w}	Model parameters
$F(\mathbf{w})$	Objective function at point w
$F_* := F(\mathbf{w}^*)$	minimum function value at minimizer
α	learning rate
α_k	learning rate scheduler/ learning rate at epoch k
$\bar{\alpha}$	fixed learning rate
c, L	strong convexity, Lipschitz constant for $\ \cdot\ _2 = \ \cdot\ _{\mathbf{I}}$
\hat{c}, \hat{L}	strong convexity, Lipschitz constant for preconditioned case: $\ \cdot\ _{\mathbf{M}}$
$\hat{\mu}_{PL}$	PL constant for preconditioned case: $\ \cdot\ _{\mathbf{M}}$
\mathcal{B}	mini-batch of the dataset
\mathbf{M}	generic preconditioner where \mathbf{M}^{-1} is applied to a vector
$g(\cdot, \cdot)$	gradient vector
$\kappa(\mathbf{M})$	Condition number of \mathbf{M} (always based on $\ \cdot\ _2$)
μ, μ_G	lower and upper bound constants on the first moment of the gradient
K, K_V	constant and scaling values of the affine bound on the gradient's variance
K_G	Constant needed for learning rate upper bound, dependent on $K_V + \mu_G^2 > 0$.
$\mathbb{E}_{\xi}, \mathbb{V}_{\xi}$	Expectation and Variance of gradient with random realization ξ
β, γ	constants affecting the lower and upper bound on α_k for diminishing learning rate proofs
ν	convergence constant in $\mathcal{O}((\gamma + k)^{-1})$
r	radius of convex basin around local minimum
$\mathcal{N}_r, \mathcal{N}_{r+}$	local neighborhood around minimizer, slightly larger local neighborhood for containment
τ	smallest iteration number where $\mathbf{w}_k \notin \mathcal{N}_r$.
C	The stochastic noise floor defined $\bar{\alpha} \hat{L} K / (2 \hat{c} \mu)$
$\mathcal{N}_{\mathbf{M}}(\mathbf{w})$	instantaneous preconditioned noise $\text{tr}(\mathbf{M}^{-1} \Sigma(\mathbf{w}))$
K	uniform baseline for $\mathcal{N}_{\mathbf{M}}(\mathbf{w})$ on the analysis region (noise floor constant)
α_{QG}	quadratic growth constant of locally convex basin a distance from the minimizer

556 B Mathematical preliminaries

557 B.1 Preconditioning

The condition number from a linear equation $\mathbf{Ax} = \mathbf{b}$ bounds the accuracy of the solution \mathbf{x} , and is defined as

$$\kappa(\mathbf{A}) = \|\mathbf{A}\| \|\mathbf{A}^{-1}\|,$$

558 where if not stated $\|\cdot\| = \|\cdot\|_2$. If \mathbf{A} is ill-conditioned, i.e. has a large condition number, then a small
 559 perturbation in \mathbf{b} can result in a large perturbation of the solution \mathbf{x} . In addition to the accuracy of the
 560 solution, the convergence rate of iterative methods, such as conjugate gradient, depends on $r = \frac{\sqrt{\kappa}-1}{\sqrt{\kappa}+1}$.

561 It is easy to see that $r < 1$, but if $\kappa \gg 1$, then convergence will be extremely slow as $r \rightarrow 1$. This motivates
 562 the need for ways to reduce the condition number, through a technique called *preconditioning*. Throughout

563 this paper, we assume that \mathbf{M} is the preconditioner, and we only have access to the action of \mathbf{M}^{-1} onto a
 564 vector. More technically, we say \mathbf{M} is an efficient preconditioner to the matrix \mathbf{A} such that

$$\kappa(\mathbf{M}^{-1}\mathbf{A}) < \kappa(\mathbf{A}).$$

565 For clarity, even though we call \mathbf{M} the preconditioner, we don't explicitly form it. Additionally, we don't
 566 form \mathbf{M}^{-1} either but just observe the action of the preconditioner on a vector, $\mathbf{M}^{-1}\mathbf{v}$.

There are different ways we can utilize the preconditioner \mathbf{M} . First, assume \mathbf{M}^{-1} exists, then the *left* preconditioned system is

$$\mathbf{M}^{-1}(\mathbf{Ax} - \mathbf{b}) = 0.$$

Both the original linear system and the left-preconditioned system give the same solution. Additionally, we could solve the right preconditioned system

$$\mathbf{AM}^{-1}(\mathbf{Mx}) = \mathbf{b}.$$

567 This requires us to solve $\mathbf{AM}^{-1}\mathbf{y} = \mathbf{b}$ for \mathbf{y} , and then to recover the original solution, we would need to do
 568 another linear system solve $\mathbf{Mx} = \mathbf{y}$ for \mathbf{x} .

569 These two techniques can be combined to perform *split* preconditioning. If we employ \mathbf{M} as the right
 570 preconditioner, and \mathbf{N} as the left preconditioner, we compute

$$\mathbf{NAM}^{-1}(\mathbf{Mx}) = \mathbf{Nb}.$$

571 This is beneficial if one would like to scale the rows and columns of \mathbf{A} differently. Additionally, observe that
 572 if \mathbf{A} is symmetric and $\mathbf{N}^\top = \mathbf{M}^{-1}$, then \mathbf{NAM}^{-1} is also symmetric.

573 In the preconditioned version of CG (PCG), one solves the equivalent system $\mathbf{M}^{-1}\mathbf{Ax} = \mathbf{M}^{-1}\mathbf{b}$ using a similar
 574 three-term recurrence, but applied to the transformed system. The key requirement is that the preconditioner
 575 \mathbf{M} be symmetric positive definite and chosen so that $\mathbf{M}^{-1}\mathbf{A}$ has a significantly smaller condition number
 576 than \mathbf{A} itself. For practical purposes, PCG is used in matrix-free settings where only the action $\mathbf{M}^{-1}\mathbf{v}$ is
 577 required, not the explicit matrix \mathbf{M}^{-1} .

578 B.2 Preconditioners for SGD

579 In this section, we briefly review several preconditioners commonly used in the ML literature. First, if we
 580 define \mathbf{g}_k to be the sum of the squared gradients up until iteration k , we arrive at AdaGrad (Duchi et al.,
 581 2011)

$$\mathbf{M}_{\text{AdaGrad}} = \text{diag}(\sqrt{\mathbf{g}_k} + \varepsilon).$$

582 The issues with this is the gradient squared will only increase, leading to premature stopping. To counteract that, exponentially moving weighted averages are widely used in diagonal preconditioners such as
 583 Adam (Kingma & Ba, 2017) and its momentum-less counterpart RMSProp (Hinton, 2014):

$$\mathbf{M}_{\text{Adam}} = \text{diag}(\sqrt{\mathbf{s}_k} + \varepsilon),$$

585 where here \mathbf{s}_k is an exponential moving average of squared gradients, and $\varepsilon > 0$ is a small constant added for
 586 numerical stability. While computationally efficient and robust to scaling, such diagonal preconditioners fail
 587 to capture cross-parameter curvature, which may lead to suboptimal convergence in ill-conditioned problems.

588 The Hessian matrix of the loss function,

$$\mathbf{H}(\mathbf{w}) = \nabla^2 \mathcal{L}(\mathbf{w}),$$

589 captures the exact second-order structure of the problem and provides the most complete curvature information.
 590 However, computing or storing the full Hessian is typically infeasible in high-dimensional neural network
 591 (NN) models. Moreover, it is not guaranteed to be positive definite in nonconvex settings, which complicates
 592 its direct use as a preconditioner.

593 To reduce computational cost, one can approximate the Hessian using a single mini-batch, \mathcal{B} :

$$\mathbf{H}_{\mathcal{B}}(\mathbf{w}) = \nabla^2 \mathcal{L}_{\mathcal{B}}(\mathbf{w}).$$

594 This matrix is cheaper to compute and can be updated online, but suffers from high variance and may not
 595 preserve important curvature directions observed over the full dataset. While the Newton and quasi-Newton
 596 methods work well for deterministic optimization, many have provided a distinction between these and other
 597 methods for designing preconditioners in the stochastic setting (Li, 2018; Bottou et al., 2018).

598 As opposed to constructing the Hessian, an alternative is the Gauss-Newton Hessian approximation, which
 599 assumes the difference between the model and label is small in a least-squares norm. This idea was further
 600 generalized to loss functions of the form $\ell(\theta) = \sum_n a_n(b_n(\theta))$ in Schraudolph (2002). This generalized
 601 Gauss-Newton matrix (GGN), which ignores second order information of b_n , is SPD when a_n is convex even
 602 when the true Hessian is indefinite.

603 Another alternate method is the FIM defined as

$$\mathbf{F}(\mathbf{w}) = \mathbb{E}_{x,y} [\nabla_{\mathbf{w}} \log p_{\mathbf{w}}(y | x) \nabla_{\mathbf{w}} \log p_{\mathbf{w}}(y | x)^\top],$$

604 which is guaranteed to be SPD under mild regularity conditions. For models trained with exponential-family
 605 losses, the FIM coincides with the GGN (Martens, 2020; Schraudolph, 2002). Its structure allows for stable
 606 and curvature-aware preconditioning.

607 The empirical FIM estimates the expectation in the FIM using a finite mini-batch:

$$\mathbf{F}_{\text{emp}}(\mathbf{w}) = \frac{1}{|\mathcal{B}|} \sum_{(x,y) \in \mathcal{B}} \nabla_{\mathbf{w}} \log p_{\mathbf{w}}(y | x) \nabla_{\mathbf{w}} \log p_{\mathbf{w}}(y | x)^\top.$$

608 It is symmetric and positive semidefinite, and is often used in practice due to its lower computational overhead
 609 compared to the full FIM. However, it may introduce bias depending on the mini-batch size and model
 610 quality (Kunstner et al., 2019).

611 Finally, the L-BFGS algorithm is a popular quasi-Newton method that builds a low-rank approximation
 612 to the inverse Hessian using a history of gradients and iterates. It is well-suited to medium-scale problems
 613 and has seen empirical success in ML (Bottou et al., 2018). Additional variants of L-BFGS have also been
 614 proposed (Berahas et al., 2016; Bollapragada et al., 2018). While not traditionally framed as a preconditioner,
 615 L-BFGS can be interpreted as implicitly applying a data-driven curvature approximation.

616 C Assumptions and proofs of theorems

617 C.1 Assumptions

618 **Assumption 9** (Strong Convexity). *The objective function $F: \mathbb{R}^d \rightarrow \mathbb{R}$ is strongly convex in that there exists
 619 a constant $c > 0$ such that*

$$F(\bar{\mathbf{w}}) \geq F(\mathbf{w}) + \nabla F(\mathbf{w})^\top (\bar{\mathbf{w}} - \mathbf{w}) + \frac{1}{2}c\|\bar{\mathbf{w}} - \mathbf{w}\|_2^2, \quad \forall (\bar{\mathbf{w}}, \mathbf{w}) \in \mathbb{R}^d \times \mathbb{R}^d$$

620 From elementary optimization, this assumption is equivalent to F having a unique minimizer $\mathbf{w}^* \in \mathbb{R}^d$. We
 621 define $F_* := F(\mathbf{w}^*)$.

622 **Assumption 10** (Lipschitz continuity of gradient). *The objective function $F: \mathbb{R}^d \rightarrow \mathbb{R}$ is continuously
 623 differentiable and the gradient function of F , $\nabla F: \mathbb{R}^d \rightarrow \mathbb{R}^d$, is Lipschitz continuous with Lipschitz constant
 624 $L > 0$, i.e.*

$$\|\nabla F(\mathbf{w}) - \nabla F(\bar{\mathbf{w}})\|_2 \leq L\|\mathbf{w} - \bar{\mathbf{w}}\|_2$$

625 for all $\{\mathbf{w}, \bar{\mathbf{w}}\} \subset \mathbb{R}^d$.

626 **Remark 1.** If F is continuously twice differentiable, then ∇F is Lipschitz continuous with Lipschitz constant
 627 L if and only if the eigenvalues of the matrix $\nabla^2 F(\mathbf{w})$ are bounded above by L for all \mathbf{w} . F is strongly convex
 628 with constant c if and only if the eigenvalues of the matrix $\nabla^2 F(\mathbf{w})$ is bounded below by c for all \mathbf{w} . Therefore,
 629 L/c is an upper bound of the condition number of $\nabla^2 F(\mathbf{w})$.

630 Lipschitz continuity of gradient is an assumption made in nearly all convergence analyses of gradient-based
 631 methods (Khaled & Richtárik, 2023).

632 **Assumption 11** (Bounds on First and Second Moments of Gradient). *Assume*

633 1. *There exist scalars $\mu_G \geq \mu > 0$ such that, for all $k \in \mathbb{N}$,*

$$\nabla F(\mathbf{w}_k)^\top \mathbb{E}_{\xi_k}[g(\mathbf{w}_k, \xi_k)] \geq \mu \|\nabla F(\mathbf{w}_k)\|_2^2 \quad (9)$$

$$\|\mathbb{E}_{\xi_k}[g(\mathbf{w}_k, \xi_k)]\|_2 \leq \mu_G \|\nabla F(\mathbf{w}_k)\|_2 \quad (10)$$

635 2. *There exist scalars $K \geq 0$ and $K_V \geq 0$ such that, for all $k \in \mathbb{N}$,*

$$\mathbb{V}_{\xi_k}[g(\mathbf{w}_k, \xi_k)] \leq K + K_V \|\nabla F(\mathbf{w}_k)\|_2^2 \quad (11)$$

636 where $\mathbb{V}_{\xi_k}[g(\mathbf{w}_k, \xi_k)] := \mathbb{E}_{\xi_k}[\|g(\mathbf{w}_k, \xi_k)\|_2^2] - \|\mathbb{E}_{\xi_k}[g(\mathbf{w}_k, \xi_k)]\|_2^2$.

637 **Theorem C.1** (Strongly convex objective function, fixed learning rate (Bottou et al., 2018)). *Under
 638 Assumptions 9, 10, 11, suppose that the SGD algorithm is run with fixed learning rates, $\alpha_k = \bar{\alpha}$ for all $k \in \mathbb{N}$
 639 where*

$$0 < \bar{\alpha} \leq \frac{\mu}{LK_G} \quad \text{and} \quad K_G := K_V + \mu_G^2 \geq \mu^2 > 0.$$

640 *Then, the expected optimality gap satisfies the following for all $k \in \mathbb{N}$:*

$$\mathbb{E}[F(\mathbf{w}_k) - F_*] \leq \frac{\bar{\alpha}LK}{2c\mu} + (1 - \bar{\alpha}c\mu)^{k-1} \left(F(\mathbf{w}_1) - F_* - \frac{\bar{\alpha}LK}{2c\mu} \right) \xrightarrow{k \rightarrow \infty} \frac{\bar{\alpha}LK}{2c\mu} \quad (12)$$

641 Note that it follows from (10) and (11) that $\mathbb{E}_{\xi_k}[\|g(\mathbf{w}_k, \xi_k)\|_2^2] \leq K + K_G \|\nabla F(\mathbf{w}_k)\|_2^2$ with $K_G := K_V + \mu_G^2 \geq \mu^2 > 0$.

643 **Theorem C.2** (Strongly convex objective function, diminishing learning rates (Bottou et al., 2018)). *Under
 644 the same assumptions as Theorem C.1, suppose that the SGD algorithm is run with a learning rate sequence
 645 such that, for all $k \in \mathbb{N}$,*

$$\alpha_k = \frac{\beta}{\gamma + k} \text{ for some } \beta > \frac{1}{c\mu} \text{ and } \gamma > 0 \text{ such that } \alpha_1 \leq \frac{\mu}{LK_G}$$

646 *Then, the expected optimality gap satisfies the following for all $k \in \mathbb{N}$:*

$$\mathbb{E}[F(\mathbf{w}_k) - F_*] \leq \frac{\nu}{\gamma + k} \quad (13)$$

647 *where*

$$\nu := \max \left\{ \frac{\beta^2 LK}{2(\beta c\mu - 1)}, (\gamma + 1)(F(\mathbf{w}_1) - F_*) \right\} \quad (14)$$

648 Under the assumption of strong convexity, the optimality gap can be bounded at any point by the 2-norm
 649 squared of the gradient of the objective function at that particular point. That is,

$$2c(F(\mathbf{w}) - F_*) \leq \|\nabla F(\mathbf{w})\|_2^2 \text{ for all } \mathbf{w} \in \mathbb{R}^d$$

650 As before, F has a unique minimizer, denoted as $\mathbf{w}^* \in \mathbb{R}^d$ with $F_* := F(\mathbf{w}^*)$.

651 Previously, the optimality gap was bounded by the 2-norm of the gradient of the objective function squared.
 652 Here, however, the optimality gap is bounded by the \mathbf{M} -norm of the gradient of the objective function squared.
 653 That is,

$$2\hat{c}(F(\mathbf{w}) - F(\mathbf{w}_*)) \leq \|\nabla F(\mathbf{w})\|_{\mathbf{M}^{-1}}^2$$

654 This result is used several times in the upcoming proofs. We repeat Lemma 3.1 here for convenience below:

655 **Lemma C.3.** Let F be twice differentiable and $\mathbf{M}^{-1} = \mathbf{P}\mathbf{P}^\top$. Then: (i) ∇F is \mathbf{M} -Lipschitz with constant
 656 $\hat{L} \iff$ all eigenvalues of $\mathbf{P}^\top \nabla^2 F(\mathbf{w}) \mathbf{P}$ are $\leq \hat{L}$; (ii) F is \mathbf{M} -strongly convex with constant $\hat{c} \iff$ all
 657 eigenvalues of $\mathbf{P}^\top \nabla^2 F(\mathbf{w}) \mathbf{P}$ are $\geq \hat{c}$.

658 *Proof.* We consider a change of parameter as used in preconditioning. Let $\mathbf{w} = \mathbf{P}\mathbf{z}$ and $\bar{\mathbf{w}} = \mathbf{P}\bar{\mathbf{z}}$. Then
 659 $\mathbf{w} - \bar{\mathbf{w}} = \mathbf{P}(\mathbf{z} - \bar{\mathbf{z}})$ which gives $\mathbf{P}^{-1}(\mathbf{w} - \bar{\mathbf{w}}) = \mathbf{z} - \bar{\mathbf{z}}$. Define $f(\mathbf{z}) = F(\mathbf{P}\mathbf{z})$. Then $\nabla_{\mathbf{z}} f(\mathbf{z}) = \mathbf{P}^\top \nabla_{\mathbf{w}} F(\mathbf{w})$ and
 660 $\nabla_{\mathbf{z}}^2 f(z) = \mathbf{P}^\top \nabla_{\mathbf{w}}^2 F(\mathbf{w}) \mathbf{P}$. Hence

$$\|\nabla f(\mathbf{z}) - \nabla f(\bar{\mathbf{z}})\|_2 = \|\mathbf{P}^\top \nabla_{\mathbf{w}} F(\mathbf{w}) - \mathbf{P}^\top \nabla_{\mathbf{w}} F(\bar{\mathbf{w}})\|_2 = \|\nabla_{\mathbf{w}} F(\mathbf{w}) - \nabla_{\mathbf{w}} F(\bar{\mathbf{w}})\|_{\mathbf{M}^{-1}}.$$

661 Therefore, the \mathbf{M} -Lipschitz continuity of the gradient for F is equivalent to the Lipschitz continuity of the
 662 gradient for f , which is equivalent to that $\nabla_{\mathbf{z}}^2 f(z)$, i.e. $\mathbf{P}^\top \nabla_{\mathbf{w}}^2 F(\mathbf{w}) \mathbf{P}$, has eigenvalues bounded above by \hat{L} .
 663 Similarly, the statement on \mathbf{M} -strong convexity follows from

$$F(\mathbf{w}) + \nabla F(\mathbf{w})^\top (\bar{\mathbf{w}} - \mathbf{w}) + \frac{1}{2}\hat{c}\|\bar{\mathbf{w}} - \mathbf{w}\|_{\mathbf{M}}^2 = f(\mathbf{z}) + \nabla_{\mathbf{z}} f(\mathbf{z})^\top (\bar{\mathbf{z}} - \mathbf{z}) + \frac{1}{2}\hat{c}\|\bar{\mathbf{z}} - \mathbf{z}\|_2^2.$$

664

□

665 We may assume \hat{L} and \hat{c} are respectively the maximum and the minimum of the eigenvalues of $\mathbf{P}^\top \nabla^2 F(\mathbf{w}) \mathbf{P}$
 666 for all \mathbf{w} . So $\frac{\hat{L}}{\hat{c}}$ plays the role of the condition number of the preconditioned matrix $\mathbf{P}^\top \nabla^2 F(\mathbf{w}) \mathbf{P}$. If we
 667 assume $\mathbf{M}^{-1} = \mathbf{P}\mathbf{P}^\top$ is such that $\frac{\hat{L}}{\hat{c}}$ is smaller than $\frac{L}{c}$, it basically reduces the condition number. We will
 668 demonstrate that this accelerates the speed of convergence.

669 An important lemma comes directly from this assumption.

670 **Lemma C.4.** Under the assumption of \mathbf{M} -Lipschitz continuity of gradient,

$$F(\mathbf{w}) \leq F(\bar{\mathbf{w}}) + \nabla F(\bar{\mathbf{w}})^\top (\mathbf{w} - \bar{\mathbf{w}}) + \frac{1}{2}\hat{L}\|\mathbf{w} - \bar{\mathbf{w}}\|_{\mathbf{M}}^2 \quad (15)$$

Proof. Consider the following,

$$\begin{aligned} F(\mathbf{w}) &= F(\bar{\mathbf{w}}) + \int_0^1 (\nabla F(\bar{\mathbf{w}} + t(\mathbf{w} - \bar{\mathbf{w}}))^\top \mathbf{P}\mathbf{P}^{-1}(\mathbf{w} - \bar{\mathbf{w}})) \, dt \\ &= F(\bar{\mathbf{w}}) + \nabla F(\bar{\mathbf{w}})^\top (\mathbf{w} - \bar{\mathbf{w}}) + \int_0^1 (\nabla F(\bar{\mathbf{w}} + t(\mathbf{w} - \bar{\mathbf{w}})) - \nabla F(\bar{\mathbf{w}}))^\top \mathbf{P}\mathbf{P}^{-1}(\mathbf{w} - \bar{\mathbf{w}}) \, dt \\ &\leq F(\bar{\mathbf{w}}) + \nabla F(\bar{\mathbf{w}})^\top (\mathbf{w} - \bar{\mathbf{w}}) + \int_0^1 \hat{L}\|t(\mathbf{w} - \bar{\mathbf{w}})\|_{\mathbf{M}}\|\mathbf{w} - \bar{\mathbf{w}}\|_{\mathbf{M}} \, dt \end{aligned}$$

671 which gives us our consequence that was to be shown. □

672 Notice that combining the variance definition (Eq. 3) with Assumption 3, we have the following

$$\mathbb{E}_{\xi_k}[\|g(\mathbf{w}_k, \xi_k)\|_{\mathbf{M}^{-1}}^2] \leq K_G \|\nabla F(\mathbf{w}_k)\|_{\mathbf{M}^{-1}}^2 + K \text{ with } K_G := K_V + \mu_G^2 \geq \mu^2 > 0 \quad (16)$$

673 The proof for the two theorems relies on the following lemmas.

674 **Lemma C.5.** Under Assumption 1, the iterates of Eq. 2 satisfy the following inequality for all $k \in \mathbb{N}$:

$$\mathbb{E}_{\xi_k}[F(\mathbf{w}_{k+1})] - F(\mathbf{w}_k) \leq -\alpha_k \nabla F(\mathbf{w}_k)^\top \mathbb{E}_{\xi_k}[g(\mathbf{w}_k, \xi_k)] + \frac{1}{2}\alpha_k^2 \hat{L} \mathbb{E}_{\xi_k}[\|g(\mathbf{w}_k, \xi_k)\|_{\mathbf{M}^{-1}}^2] \quad (17)$$

675 *Proof.* Let $\mathbf{w} = \mathbf{w}_{k+1}$ and $\bar{\mathbf{w}} = \mathbf{w}_k$. Then, by Assumption 1,

$$F(\mathbf{w}_{k+1}) - F(\mathbf{w}_k) \leq \nabla F(\mathbf{w}_k)^\top (\mathbf{w}_{k+1} - \mathbf{w}_k) + \frac{1}{2}\hat{L}\|\mathbf{w}_{k+1} - \mathbf{w}_k\|_{\mathbf{M}}^2$$

Recalling that Eq. 2 gives $\mathbf{w}_{k+1} = \mathbf{w}_k - \alpha_k \mathbf{M}^{-1} g(\mathbf{w}_k, \boldsymbol{\xi}_k)$, we then have,

$$\begin{aligned} F(\mathbf{w}_{k+1}) - F(\mathbf{w}_k) &\leq \nabla F(\mathbf{w}_k)^\top (-\alpha_k \mathbf{M}^{-1} g(\mathbf{w}_k, \boldsymbol{\xi}_k)) + \frac{1}{2} \hat{L} \|\alpha_k \mathbf{M}^{-1} g(\mathbf{w}_k, \boldsymbol{\xi}_k)\|_{\mathbf{M}}^2 \\ &\leq -\alpha_k \nabla F(\mathbf{w}_k)^\top \mathbf{M}^{-1} g(\mathbf{w}_k, \boldsymbol{\xi}_k) + \frac{1}{2} \alpha_k^2 \hat{L} \|\mathbf{M}^{-1} g(\mathbf{w}_k, \boldsymbol{\xi}_k)\|_{\mathbf{M}}^2 \\ &\leq -\alpha_k \nabla F(\mathbf{w}_k)^\top \mathbf{M}^{-1} g(\mathbf{w}_k, \boldsymbol{\xi}_k) + \frac{1}{2} \alpha_k^2 \hat{L} \|g(\mathbf{w}_k, \boldsymbol{\xi}_k)\|_{\mathbf{M}^{-1}}^2 \end{aligned}$$

676 Take the expectation of both sides

$$\mathbb{E}_{\boldsymbol{\xi}_k}[F(\mathbf{w}_{k+1})] - F(\mathbf{w}_k) \leq -\alpha_k \nabla F(\mathbf{w}_k)^\top \mathbf{M}^{-1} \mathbb{E}_{\boldsymbol{\xi}_k}[g(\mathbf{w}_k, \boldsymbol{\xi}_k)] + \frac{1}{2} \alpha_k^2 \hat{L} \mathbb{E}_{\boldsymbol{\xi}_k}[\|g(\mathbf{w}_k, \boldsymbol{\xi}_k)\|_{\mathbf{M}^{-1}}^2]$$

677 Thus, the desired result is achieved. \square

Lemma C.6. *Under Assumptions 1 and 2, the iterates of Eq. 2 satisfy the following inequalities for all $k \in \mathbb{N}$:*

$$\mathbb{E}_{\boldsymbol{\xi}_k}[F(\mathbf{w}_{k+1})] - F(\mathbf{w}_k) \leq -\mu \alpha_k \|\nabla F(\mathbf{w}_k)\|_{\mathbf{M}^{-1}}^2 + \frac{1}{2} \alpha_k^2 \hat{L} \mathbb{E}_{\boldsymbol{\xi}_k}[\|g(\mathbf{w}_k, \boldsymbol{\xi}_k)\|_{\mathbf{M}^{-1}}^2] \quad (18)$$

$$\leq -(\mu - \frac{1}{2} \alpha_k \hat{L} K_G) \alpha_k \|\nabla F(\mathbf{w}_k)\|_{\mathbf{M}^{-1}}^2 + \frac{1}{2} \alpha_k^2 \hat{L} K \quad (19)$$

Proof. By Lemma C.5 and Assumption 2, it follows that

$$\begin{aligned} \mathbb{E}_{\boldsymbol{\xi}_k}[F(\mathbf{w}_{k+1})] - F(\mathbf{w}_k) &\leq -\alpha_k \mu \|\nabla F(\mathbf{w}_k)\|_{\mathbf{M}^{-1}}^2 + \frac{1}{2} \alpha_k^2 \hat{L} \mathbb{E}_{\boldsymbol{\xi}_k}[\|g(\mathbf{w}_k, \boldsymbol{\xi}_k)\|_{\mathbf{M}^{-1}}^2] \\ &\leq -\alpha_k \mu \|\nabla F(\mathbf{w}_k)\|_{\mathbf{M}^{-1}}^2 + \frac{1}{2} \alpha_k^2 \hat{L} (K_G \|\nabla F(\mathbf{w}_k)\|_{\mathbf{M}^{-1}}^2 + K) \\ &\leq -\left(\mu - \frac{1}{2} \alpha_k \hat{L} K_G\right) \alpha_k \|\nabla F(\mathbf{w}_k)\|_{\mathbf{M}^{-1}}^2 + \frac{1}{2} \alpha_k^2 \hat{L} K \end{aligned}$$

678 Hence, we have the desired inequalities. \square

679 The final lemma necessary is as follows.

680 **Lemma C.7.** *Under assumptions 1, 2, and 3 (with F_* being the minimum of F), suppose Eq. 2 is run with
681 a learning rate sequence such that for all $k \in \mathbb{N}$, assume $\alpha_k \leq \frac{\mu}{\hat{L} K_G}$. (Note that α_k could be constant for all
682 $k \in \mathbb{N}$). Then the following inequality holds*

$$\mathbb{E}[F(\mathbf{w}_{k+1}) - F_*] \leq (1 - \alpha_k \hat{\mu}) \mathbb{E}[F(\mathbf{w}_k) - F_*] + \frac{1}{2} \alpha_k^2 \hat{L} K \quad (20)$$

Proof. Given the assumptions and using Lemma C.6, we have $\mathbb{E}_{\boldsymbol{\xi}_k}[F(\mathbf{w}_{k+1})] - F(\mathbf{w}_k) \leq -\hat{\mu} \alpha_k (F(\mathbf{w}_k) - F_*) + \frac{1}{2} \alpha_k^2 \hat{L} K$. Subtract F_* from both sides and take the total expectation. We denote this total expectation as $\mathbb{E}[\cdot]$, which represents the expected value taken with respect to all random variables. That is, $\mathbb{E}[F(\mathbf{w}_k)] = \mathbb{E}_{\xi_1} \mathbb{E}_{\xi_2} \dots \mathbb{E}_{\xi_{k-1}}[F(\mathbf{w}_k)]$.

$$\begin{aligned} \mathbb{E}[\mathbb{E}_{\boldsymbol{\xi}_k}[F(\mathbf{w}_{k+1})] - F(\mathbf{w}_k) - F_*] &\leq \mathbb{E} \left[-\hat{\mu} \alpha_k (F(\mathbf{w}_k) - F_*) + \frac{1}{2} \alpha_k^2 \hat{L} K - F_* \right] \\ \mathbb{E}[\mathbb{E}_{\boldsymbol{\xi}_k}[F(\mathbf{w}_{k+1})] - F_*] &\leq \mathbb{E}[-\hat{\mu} \alpha_k (F(\mathbf{w}_k) - F_*) - F(\mathbf{w}_k) - F_*] + \frac{1}{2} \alpha_k^2 \hat{L} K \\ &\leq \mathbb{E}[-\hat{\mu} \alpha_k F(\mathbf{w}_k) + \hat{\mu} \alpha_k F_* + F(\mathbf{w}_k) - F_*] + \frac{1}{2} \alpha_k^2 \hat{L} K \\ &\leq (1 - \hat{\mu} \alpha_k) \mathbb{E}[F(\mathbf{w}_k) - F_*] + \frac{1}{2} \alpha_k^2 \hat{L} K \end{aligned}$$

683 which is our desired inequality (20). \square

684 **C.2 Proofs of main theorems**685 **C.2.1 Proof of Theorem 3.2**

Proof. Using Lemma C.6, we have for all $k \in \mathbb{N}$:

$$\begin{aligned}\mathbb{E}_{\xi_k}[F(\mathbf{w}_{k+1})] - F(\mathbf{w}_k) &\leq -(\mu - \frac{1}{2}\bar{\alpha}\hat{L}K_G)\bar{\alpha}\|\nabla F(\mathbf{w}_k)\|_{\mathbf{M}^{-1}}^2 + \frac{1}{2}\bar{\alpha}^2\hat{L}K \\ &\leq -\left(\mu - \frac{1}{2}\left(\frac{\mu}{\hat{L}K_G}\right)\hat{L}K_G\right)\bar{\alpha}\|\nabla F(\mathbf{w}_k)\|_{\mathbf{M}^{-1}}^2 + \frac{1}{2}\bar{\alpha}^2\hat{L}K \\ &= -\frac{1}{2}\bar{\alpha}\mu\|\nabla F(\mathbf{w}_k)\|_{\mathbf{M}^{-1}}^2 + \frac{1}{2}\bar{\alpha}^2\hat{L}K \\ &\leq -\frac{1}{2}\bar{\alpha}\mu[2\hat{c}(F(\mathbf{w}_k) - F(\mathbf{w}_*))] + \frac{1}{2}\bar{\alpha}^2\hat{L}K \\ &\leq -\bar{\alpha}\hat{c}\mu(F(\mathbf{w}_k) - F_*) + \frac{1}{2}\bar{\alpha}^2\hat{L}K\end{aligned}$$

Now, subtract the constant $\frac{\bar{\alpha}\hat{L}K}{2\hat{c}\mu}$ from both sides of inequality (Eq. 20)

$$\mathbb{E}[F(\mathbf{w}_{k+1}) - F_*] - \frac{\bar{\alpha}\hat{L}K}{2\hat{c}\mu} \leq (1 - \bar{\alpha}\hat{c}\mu)\mathbb{E}[F(\mathbf{w}_k) - F_*] + \frac{1}{2}\bar{\alpha}\hat{L}K - \frac{\bar{\alpha}\hat{L}K}{2\hat{c}\mu} \quad (21)$$

$$= (1 - \bar{\alpha}\hat{c}\mu) \left(\mathbb{E}[F(\mathbf{w}_k) - F_*] - \frac{\bar{\alpha}\hat{L}K}{2\hat{c}\mu} \right) \quad (22)$$

686 We must now notice the following chain of inequalities.

$$0 < \bar{\alpha}\hat{c}\mu \leq \frac{\hat{c}\mu^2}{\hat{L}K_G}$$

687 This inequality holds by the theorem assumption that $0 < \bar{\alpha} \leq \frac{\mu}{\hat{L}K_G}$.

$$\frac{\hat{c}\mu^2}{\hat{L}K_G} \leq \frac{\hat{c}\mu^2}{\hat{L}\mu^2} = \frac{\hat{c}}{\hat{L}}$$

688 This inequality holds by (16) from Assumption 3.

689 Now, note that since $\hat{c} \leq \hat{L}$, it follows that $\frac{\hat{c}}{\hat{L}} \leq 1$. The result thus follows by applying C.6 repeatedly through 690 iteration $k \in \mathbb{N}$. \square

691 **Corollary C.7.1.** *If $g(\mathbf{w}_k, \xi_k)$ is an unbiased estimate of $\nabla F(\mathbf{w}_k)$, and the variance of $g(\mathbf{w}_k, \xi_k)$ is bounded 692 by a constant K independent of $\nabla F(\mathbf{w}_k)$, Then for a fixed learning rate bounded by $\frac{K_G}{\hat{L}K_G}$, $\mathbb{E}[F(\mathbf{w}_k) - F_*]$ 693 decreases to below $\frac{\bar{\alpha}\hat{L}K}{2\hat{c}\mu}$ at the rate of $\frac{\hat{c}}{\hat{L}}$.*

694 **C.2.2 Proof of Theorem 3.3**

Proof. Since the learning rates are diminishing and by the theorem statement, we have $\alpha_k \hat{L}K_G \leq \alpha_1 \hat{L}K_G \leq \mu$ for all $k \in \mathbb{N}$. By Lemma C.6 and Assumption 3,

$$\begin{aligned}\mathbb{E}_{\xi_k}[F(\mathbf{w}_{k+1})] - F(\mathbf{w}_k) &\leq -(\mu - \frac{1}{2}\alpha_k \hat{L}K_G)\alpha_k\|\nabla F(\mathbf{w}_k)\|_{\mathbf{M}^{-1}}^2 + \frac{1}{2}\alpha_k^2\hat{L}K \\ &\leq -(\mu - \frac{1}{2}\mu)\alpha_k\|\nabla F(\mathbf{w}_k)\|_{\mathbf{M}^{-1}}^2 + \frac{1}{2}\alpha_k^2\hat{L}K \\ &\leq -\alpha_k\mu\hat{c}(F(\mathbf{w}_k) - F_*) + \frac{1}{2}\alpha_k^2\hat{L}K\end{aligned}$$

By Lemma C.7, using (20), we have

$$\mathbb{E}[F(\mathbf{w}_{k+1}) - F_*] \leq (1 - \alpha_k \hat{c}\mu) \mathbb{E}[F(\mathbf{w}_k) - F_*] + \frac{1}{2} \alpha_k^2 \hat{L}K$$

695 Now, we prove the convergence result via induction. Consider the base case, $k = 1$.

696 Since $\nu \geq (\gamma + 1)(F(\mathbf{w}_1) - F_*)$ and $\nu \geq \frac{\beta^2 \hat{L}K}{2(\beta \hat{c}\mu - 1)}$, it follows that $\mathbb{E}[F(\mathbf{w}_1) - F_*] \leq \frac{\nu}{\gamma + 1}$.

Now, we assume that (8) holds for some $k \geq 1$. Thus

$$\begin{aligned} \mathbb{E}[F(\mathbf{w}_{k+1}) - F_*] &\leq (1 - \alpha_k \hat{c}\mu) \mathbb{E}[F(\mathbf{w}_k) - F_*] + \frac{1}{2} \alpha_k^2 \hat{L}K \\ &\leq (1 - \alpha_k \hat{c}\mu) \frac{\nu}{\gamma + k} + \frac{1}{2} \alpha_k^2 \hat{L}K \\ &= \left(1 - \frac{\beta}{\gamma + k} \hat{c}\mu\right) \frac{\nu}{\gamma + k} + \frac{1}{2} \left(\frac{\beta}{\gamma + k}\right)^2 \hat{L}K \\ &= \left(1 - \frac{\beta \hat{c}\mu}{\tilde{k}}\right) \frac{\nu}{\tilde{k}} + \frac{\beta^2 \hat{L}K}{2\tilde{k}^2} \\ &= \left(\frac{\tilde{k} - 1}{\tilde{k}^2}\right) \nu - \left(\frac{\beta \hat{c}\mu - 1}{\tilde{k}^2}\right) \nu + \frac{\beta^2 \hat{L}K}{2\tilde{k}^2} \end{aligned}$$

697 where $\tilde{k} := \gamma + k$. Note that $\left(\frac{\beta \hat{c}\mu - 1}{\tilde{k}^2}\right) \nu - \frac{\beta^2 \hat{L}K}{2\tilde{k}^2} \geq 0$ since $\nu \geq \frac{\beta^2 \hat{L}K}{2(\beta \hat{c}\mu - 1)}$.

698 Thus,

$$\mathbb{E}[F(\mathbf{w}_{k+1}) - F_*] \leq \left(\frac{\tilde{k} - 1}{\tilde{k}^2}\right) \nu - \left(\frac{\beta \hat{c}\mu - 1}{\tilde{k}^2}\right) \nu + \frac{\beta \hat{L}K}{2\tilde{k}^2} \stackrel{\dagger}{\leq} \frac{\nu}{\tilde{k} + 1}$$

699 where (\dagger) follows since $\tilde{k}^2 \geq (\tilde{k} + 1)(\tilde{k} - 1)$. □

700 C.2.3 Proof of Lemma 3.4

701 *Proof.* Fix $k \leq T - 1$ and assume $\mathbf{w}_k \in \mathcal{N}_r$, i.e. $\text{dist}_{\mathbf{M}}(\mathbf{w}_k, \mathcal{S}) \leq r$. If $\mathbf{w}_{k+1} \notin \mathcal{N}_{r+}$ then $\text{dist}_{\mathbf{M}}(\mathbf{w}_{k+1}, \mathcal{S}) > r_+ = r + \Delta$. By the triangle inequality,

$$\text{dist}_{\mathbf{M}}(\mathbf{w}_{k+1}, \mathcal{S}) \leq \text{dist}_{\mathbf{M}}(\mathbf{w}_k, \mathcal{S}) + \|\mathbf{w}_{k+1} - \mathbf{w}_k\|_{\mathbf{M}} \leq r + \|\mathbf{w}_{k+1} - \mathbf{w}_k\|_{\mathbf{M}},$$

703 hence $\|\mathbf{w}_{k+1} - \mathbf{w}_k\|_{\mathbf{M}} > \Delta$. Using $\mathbf{w}_{k+1} - \mathbf{w}_k = -\alpha_k \mathbf{M}^{-1} g_k$ we have $\|\mathbf{w}_{k+1} - \mathbf{w}_k\|_{\mathbf{M}} = \alpha_k \|g_k\|_{\mathbf{M}^{-1}}$, so

$$\mathbb{P}(\mathbf{w}_{k+1} \notin \mathcal{N}_{r+} \mid \mathcal{F}_k) \leq \mathbb{P}(\alpha_k \|g_k\|_{\mathbf{M}^{-1}} > \Delta \mid \mathcal{F}_k).$$

704 Markov's inequality and Assumption 8 yield

$$\mathbb{P}(\alpha_k \|g_k\|_{\mathbf{M}^{-1}} > \Delta \mid \mathcal{F}_k) \leq \frac{\alpha_k^2 \mathbb{E}[\|g_k\|_{\mathbf{M}^{-1}}^2 \mid \mathcal{F}_k]}{\Delta^2} \leq \delta_k.$$

705 □

706 C.2.4 Proof of Theorem 3.5

707 *Proof.* Fix $\alpha_k = \bar{\alpha}$ and let $\mathcal{F}_k := \sigma(\xi_1, \dots, \xi_{k-1})$. Write $g_k := g(\mathbf{w}_k, \xi_k)$ and define

$$\tau := \inf\{k \geq 1 : \mathbf{w}_k \notin \mathcal{N}_r\}, \quad \Omega_T := \{\tau > T\}.$$

708 Fix $k \leq T - 1$ and work on Ω_T . Then $\mathbf{w}_k, \mathbf{w}_{k+1} \in \mathcal{N}_r \subset \mathcal{N}_{r+} \subset \mathcal{V}$. By convexity of \mathcal{V} , the segment
709 $[\mathbf{w}_k, \mathbf{w}_{k+1}] \subset \mathcal{V}$, and by Assumption 5 (local \mathbf{M} -smoothness),

$$F(\mathbf{w}_{k+1}) \leq F(\mathbf{w}_k) - \bar{\alpha} \nabla F(\mathbf{w}_k)^\top \mathbf{M}^{-1} g_k + \frac{\hat{L}}{2} \bar{\alpha}^2 \|g_k\|_{\mathbf{M}^{-1}}^2 \quad \text{on } \Omega_T. \quad (23)$$

Taking conditional expectation given $(\mathcal{F}_k, \Omega_T)$ and using the conditional-moment version of Assumption 6 on Ω_T yields

$$\begin{aligned}\mathbb{E}[F(\mathbf{w}_{k+1}) - F_* | \mathcal{F}_k, \Omega_T] &\leq (F(\mathbf{w}_k) - F_*) - \bar{\alpha} \mu \|\nabla F(\mathbf{w}_k)\|_{\mathbf{M}^{-1}}^2 \\ &\quad + \frac{\hat{L}}{2} \bar{\alpha}^2 (K_G \|\nabla F(\mathbf{w}_k)\|_{\mathbf{M}^{-1}}^2 + K).\end{aligned}$$

710 Using $\bar{\alpha} \leq \mu/(\hat{L}K_G)$ gives $\bar{\alpha}\mu - \frac{\hat{L}}{2}\bar{\alpha}^2 K_G \geq \frac{\mu}{2}\bar{\alpha}$, hence

$$\mathbb{E}[F(\mathbf{w}_{k+1}) - F_* | \mathcal{F}_k, \Omega_T] \leq (F(\mathbf{w}_k) - F_*) - \frac{\mu}{2}\bar{\alpha} \|\nabla F(\mathbf{w}_k)\|_{\mathbf{M}^{-1}}^2 + \frac{\hat{L}}{2}\bar{\alpha}^2 K. \quad (24)$$

711 On Ω_T we have $\mathbf{w}_k \in \mathcal{N}_r$, so Assumption 4 implies $\|\nabla F(\mathbf{w}_k)\|_{\mathbf{M}^{-1}}^2 \geq 2\hat{\mu}_{\text{PL}}(F(\mathbf{w}_k) - F_*)$. Substituting into 712 (24) gives

$$\mathbb{E}[F(\mathbf{w}_{k+1}) - F_* | \mathcal{F}_k, \Omega_T] \leq (1 - \rho)(F(\mathbf{w}_k) - F_*) + \rho C,$$

713 with $\rho := \bar{\alpha}\hat{\mu}_{\text{PL}}\mu \in (0, 1)$ and $C := \frac{\bar{\alpha}\hat{L}K}{2\hat{\mu}_{\text{PL}}\mu}$. Taking expectations under $\mathbb{P}(\cdot | \Omega_T)$ and defining $x_k :=$ 714 $\mathbb{E}[F(\mathbf{w}_k) - F_* | \Omega_T]$ yields for $k \leq T - 1$,

$$x_{k+1} \leq (1 - \rho)x_k + \rho C.$$

715 Iterating gives, for all $1 \leq k \leq T$,

$$x_k \leq C + (1 - \rho)^{k-1}(F(\mathbf{w}_1) - F_* - C),$$

716 which is the desired conditional geometric bound.

717 Define overshoot events

$$A_k := \{\mathbf{w}_k \in \mathcal{N}_r, \mathbf{w}_{k+1} \notin \mathcal{N}_{r+}\}, \quad k = 1, \dots, T-1,$$

718 and the no-overshoot event $\mathcal{E}_T := \bigcap_{k=1}^{T-1} A_k^c$. By Lemma 3.4, $\mathbb{P}(A_k) \leq \delta_k$, hence by the union bound

$$\mathbb{P}(\mathcal{E}_T^c) \leq \sum_{k=1}^{T-1} \delta_k. \quad (25)$$

719 Let $\sigma := \tau \wedge T$. On $\mathcal{E}_T \cap \{\tau \leq T\}$ we have $\mathbf{w}_\tau \in \mathcal{N}_{r+} \setminus \mathcal{N}_r$, hence by Assumption 7,

$$F(\mathbf{w}_\tau) - F_* \geq B := \frac{\alpha_{\text{QG}}}{2} r^2.$$

720 Since $\mathbf{w}_\sigma = \mathbf{w}_\tau$ on $\{\tau \leq T\}$,

$$B \mathbf{1}_{\{\tau \leq T\}} \mathbf{1}_{\mathcal{E}_T} \leq (F(\mathbf{w}_\sigma) - F_*) \mathbf{1}_{\mathcal{E}_T}.$$

721 Taking expectations gives

$$B \mathbb{P}(\tau \leq T, \mathcal{E}_T) \leq \mathbb{E}[(F(\mathbf{w}_\sigma) - F_*) \mathbf{1}_{\mathcal{E}_T}]. \quad (26)$$

722 We upper bound the RHS of (26). For each $k = 1, \dots, T-1$, define the prefix no-overshoot event

$$\mathcal{E}_{k+1} := \bigcap_{j=1}^k A_j^c,$$

723 so that $\mathcal{E}_{k+1} \in \mathcal{F}_{k+1}$ and $\mathcal{E}_T \subseteq \mathcal{E}_{k+1}$. On $\mathcal{E}_{k+1} \cap \{k < \tau\}$ we have $\mathbf{w}_k \in \mathcal{N}_r$ and $\mathbf{w}_{k+1} \in \mathcal{N}_{r+} \subset \mathcal{V}$, so by 724 smoothness,

$$F(\mathbf{w}_{k+1}) - F(\mathbf{w}_k) \leq -\bar{\alpha} \nabla F(\mathbf{w}_k)^\top \mathbf{M}^{-1} g_k + \frac{\hat{L}}{2} \bar{\alpha}^2 \|g_k\|_{\mathbf{M}^{-1}}^2 \quad \text{on } \mathcal{E}_{k+1} \cap \{k < \tau\}.$$

725 Taking conditional expectation given \mathcal{F}_k and using Assumption 6 (valid on $\{k < \tau\}$ since then $\mathbf{w}_k \in \mathcal{N}_r$)
726 yields

$$\mathbb{E}[F(\mathbf{w}_{k+1}) - F(\mathbf{w}_k) | \mathcal{F}_k] \leq -\bar{\alpha}\mu\|\nabla F(\mathbf{w}_k)\|_{\mathbf{M}^{-1}}^2 + \frac{\hat{L}}{2}\bar{\alpha}^2(K_G\|\nabla F(\mathbf{w}_k)\|_{\mathbf{M}^{-1}}^2 + K) \leq \frac{\hat{L}}{2}\bar{\alpha}^2 K,$$

727 where the last inequality uses that the first term is nonpositive and we drop it.

Now note that $F(\mathbf{w}_\sigma) - F(\mathbf{w}_1) = \sum_{k=1}^{T-1} (F(\mathbf{w}_{k+1}) - F(\mathbf{w}_k))\mathbf{1}_{\{k < \tau\}}$ and that on \mathcal{E}_T we have $\mathcal{E}_T \subseteq \mathcal{E}_{k+1}$, hence the above bound applies on $\mathcal{E}_T \cap \{k < \tau\}$ for every $k \leq T-1$. Therefore,

$$\begin{aligned} \mathbb{E}[(F(\mathbf{w}_\sigma) - F(\mathbf{w}_1))\mathbf{1}_{\mathcal{E}_T}] &= \sum_{k=1}^{T-1} \mathbb{E}[(F(\mathbf{w}_{k+1}) - F(\mathbf{w}_k))\mathbf{1}_{\mathcal{E}_T}\mathbf{1}_{\{k < \tau\}}] \\ &= \sum_{k=1}^{T-1} \mathbb{E}[\mathbf{1}_{\mathcal{E}_T}\mathbf{1}_{\{k < \tau\}}\mathbb{E}[F(\mathbf{w}_{k+1}) - F(\mathbf{w}_k) | \mathcal{F}_k]] \\ &\leq \sum_{k=1}^{T-1} \frac{\hat{L}}{2}\bar{\alpha}^2 K = \frac{\hat{L}}{2}\bar{\alpha}^2 K(T-1), \end{aligned}$$

728 which implies

$$\mathbb{E}[(F(\mathbf{w}_\sigma) - F_*)\mathbf{1}_{\mathcal{E}_T}] \leq (F(\mathbf{w}_1) - F_*) + \frac{\hat{L}}{2}\bar{\alpha}^2 K(T-1). \quad (27)$$

729 Combining (26) and (27) yields

$$\mathbb{P}(\tau \leq T, \mathcal{E}_T) \leq \frac{F(\mathbf{w}_1) - F_* + \frac{\hat{L}}{2}\bar{\alpha}^2 K(T-1)}{B}.$$

730 Finally, using (25),

$$\mathbb{P}(\tau \leq T) \leq \mathbb{P}(\tau \leq T, \mathcal{E}_T) + \mathbb{P}(\mathcal{E}_T^c) \leq \frac{F(\mathbf{w}_1) - F_* + \frac{\hat{L}}{2}\bar{\alpha}^2 K(T-1)}{B} + \sum_{k=1}^{T-1} \delta_k,$$

731 and rearranging gives the stated lower bound on $\mathbb{P}(\tau > T)$ (with truncation at 0). \square

732 C.2.5 Proof of Theorem 3.6

733 *Proof.* Let $\mathcal{F}_k := \sigma(\xi_1, \dots, \xi_{k-1})$, set $\alpha_k = \beta/(\gamma + k)$, and write $g_k := g(\mathbf{w}_k, \xi_k)$. Define $\tau := \inf\{k \geq 1 : \mathbf{w}_k \notin \mathcal{N}_r\}$, $\Omega_T := \{\tau > T\}$, and $S_k := F(\mathbf{w}_k) - F_*$.

735 Fix $k \leq T-1$ and work on Ω_T . Then $\mathbf{w}_k, \mathbf{w}_{k+1} \in \mathcal{N}_r \subset \mathcal{N}_{r+} \subset \mathcal{V}$. Since \mathcal{V} is convex, $[\mathbf{w}_k, \mathbf{w}_{k+1}] \subset \mathcal{V}$ and
736 Assumption 5 implies the \mathbf{M} -smoothness inequality:

$$F(\mathbf{w}_{k+1}) \leq F(\mathbf{w}_k) - \alpha_k \nabla F(\mathbf{w}_k)^\top \mathbf{M}^{-1} g_k + \frac{\hat{L}}{2}\alpha_k^2 \|g_k\|_{\mathbf{M}^{-1}}^2 \quad \text{on } \Omega_T.$$

Take conditional expectation given \mathcal{F}_k and using Assumption 6 (valid on $\{k < \tau\}$ since then $\mathbf{w}_k \in \mathcal{N}_r$) yields:

$$\mathbb{E}[S_{k+1} | \mathcal{F}_k, \Omega_T] \leq S_k - \alpha_k \mu \|\nabla F(\mathbf{w}_k)\|_{\mathbf{M}^{-1}}^2 + \frac{\hat{L}}{2}\alpha_k^2 (K_G\|\nabla F(\mathbf{w}_k)\|_{\mathbf{M}^{-1}}^2 + K).$$

737 Because $\alpha_k \leq \alpha_1 = \beta/(\gamma + 1) \leq \mu/(\hat{L}K_G)$, we have $\mu\alpha_k - \frac{\hat{L}}{2}\alpha_k^2 K_G \geq \frac{\mu}{2}\alpha_k$, hence

$$\mathbb{E}[S_{k+1} | \mathcal{F}_k, \Omega_T] \leq S_k - \frac{\mu}{2}\alpha_k \|\nabla F(\mathbf{w}_k)\|_{\mathbf{M}^{-1}}^2 + \frac{\hat{L}}{2}\alpha_k^2 K.$$

738 On Ω_T we have $\mathbf{w}_k \in \mathcal{N}_r$, so Assumption 4 yields $\|\nabla F(\mathbf{w}_k)\|_{\mathbf{M}^{-1}}^2 \geq 2\hat{\mu}_{\text{PL}} S_k$. Therefore, with $m := \mu\hat{\mu}_{\text{PL}}$ and
739 $c := \hat{L}K/2$,

$$\mathbb{E}[S_{k+1} | \mathcal{F}_k, \Omega_T] \leq (1 - m\alpha_k)S_k + c\alpha_k^2.$$

⁷⁴⁰ Now take expectation under $\mathbb{P}(\cdot | \Omega_T)$ and define $x_k := \mathbb{E}[S_k | \Omega_T]$. Then for all $k \leq T-1$,

$$x_{k+1} \leq (1 - m\alpha_k)x_k + c\alpha_k^2.$$

⁷⁴¹ Substituting $\alpha_k = \beta/(\gamma + k)$ gives

$$x_{k+1} \leq \left(1 - \frac{a}{\gamma + k}\right)x_k + \frac{b}{(\gamma + k)^2}, \quad a := \beta m, \quad b := c\beta^2.$$

⁷⁴² Since $\beta > 2/(\hat{\mu}_{\text{PL}}\mu)$, we have $a > 1$. Let

$$\nu := \max\left\{\frac{b}{a-1}, (\gamma+1)x_1\right\}, \quad x_1 = F(\mathbf{w}_1) - F_*.$$

⁷⁴³ We prove by induction that $x_k \leq \nu/(\gamma + k)$ for $1 \leq k \leq T$. The base case holds because $x_1 \leq \nu/(\gamma + 1)$ by ⁷⁴⁴ definition of ν . Assuming $x_k \leq \nu/(\gamma + k)$, we obtain

$$x_{k+1} \leq \left(1 - \frac{a}{\gamma + k}\right)\frac{\nu}{\gamma + k} + \frac{b}{(\gamma + k)^2} = \frac{\nu}{\gamma + k} + \frac{b - a\nu}{(\gamma + k)^2}.$$

⁷⁴⁵ Using $\nu \geq b/(a-1)$ implies $b - a\nu \leq -\nu$, hence

$$x_{k+1} \leq \frac{\nu}{\gamma + k} - \frac{\nu}{(\gamma + k)^2} \leq \frac{\nu}{\gamma + k} - \frac{\nu}{(\gamma + k)(\gamma + k + 1)} = \frac{\nu}{\gamma + k + 1}.$$

⁷⁴⁶ Thus $x_k \leq \nu/(\gamma + k)$ for all $1 \leq k \leq T$, i.e.

$$\mathbb{E}[F(\mathbf{w}_k) - F_* | \Omega_T] \leq \frac{\nu}{\gamma + k}, \quad 1 \leq k \leq T.$$

⁷⁴⁷ Define overshoot events $A_k := \{\mathbf{w}_k \in \mathcal{N}_r, \mathbf{w}_{k+1} \notin \mathcal{N}_{r+}\}$ for $k = 1, \dots, T-1$ and $\mathcal{E}_T := \bigcap_{k=1}^{T-1} A_k^c$. By ⁷⁴⁸ Lemma 3.4, $\mathbb{P}(A_k) \leq \delta_k$, hence

$$\mathbb{P}(\mathcal{E}_T^c) \leq \sum_{k=1}^{T-1} \delta_k.$$

⁷⁴⁹ Let $\sigma := \tau \wedge T$. On $\mathcal{E}_T \cap \{\tau \leq T\}$ we have $\mathbf{w}_\tau \in \mathcal{N}_{r+} \setminus \mathcal{N}_r$, so Assumption 7 yields

$$F(\mathbf{w}_\tau) - F_* \geq B := \frac{\alpha_{\text{QG}}}{2}r^2.$$

⁷⁵⁰ Since $\mathbf{w}_\sigma = \mathbf{w}_\tau$ on $\{\tau \leq T\}$, it follows that

$$B \mathbf{1}_{\{\tau \leq T\}} \mathbf{1}_{\mathcal{E}_T} \leq (F(\mathbf{w}_\sigma) - F_*) \mathbf{1}_{\mathcal{E}_T}.$$

⁷⁵¹ Taking expectations gives

$$B \mathbb{P}(\tau \leq T, \mathcal{E}_T) \leq \mathbb{E}[(F(\mathbf{w}_\sigma) - F_*) \mathbf{1}_{\mathcal{E}_T}].$$

⁷⁵² We upper bound the right-hand side by telescoping. For $k = 1, \dots, T-1$, define the prefix event $\mathcal{E}_k := \bigcap_{j=1}^{k-1} A_j^c$ (so $\mathcal{E}_k \in \mathcal{F}_k$ and $\mathcal{E}_T \subseteq \mathcal{E}_k$). On $\mathcal{E}_k \cap \{k < \tau\}$ we have $\mathbf{w}_k \in \mathcal{N}_r$ and $\mathbf{w}_{k+1} \in \mathcal{N}_{r+} \subset \mathcal{V}$, so the smoothness inequality and Assumption 6 imply

$$\mathbb{E}[F(\mathbf{w}_{k+1}) - F(\mathbf{w}_k) | \mathcal{F}_k] \leq c\alpha_k^2 \quad \text{on } \mathcal{E}_k \cap \{k < \tau\},$$

⁷⁵³ using again $\alpha_k \leq \mu/(\hat{L}K_G)$ to drop the (nonpositive) gradient-dependent part. Multiplying by $\mathbf{1}_{\mathcal{E}_T} \mathbf{1}_{\{k < \tau\}}$ and taking expectations yields

$$\mathbb{E}[(F(\mathbf{w}_{k+1}) - F(\mathbf{w}_k)) \mathbf{1}_{\mathcal{E}_T} \mathbf{1}_{\{k < \tau\}}] \leq c\alpha_k^2.$$

757 Summing over $k = 1, \dots, T - 1$ and using $F(\mathbf{w}_\sigma) - F(\mathbf{w}_1) = \sum_{k=1}^{T-1} (F(\mathbf{w}_{k+1}) - F(\mathbf{w}_k)) \mathbf{1}_{\{k < \tau\}}$ gives

$$\mathbb{E}[(F(\mathbf{w}_\sigma) - F(\mathbf{w}_1)) \mathbf{1}_{\mathcal{E}_T}] \leq c \sum_{k=1}^{T-1} \alpha_k^2,$$

758 hence

$$\mathbb{E}[(F(\mathbf{w}_\sigma) - F_*) \mathbf{1}_{\mathcal{E}_T}] \leq (F(\mathbf{w}_1) - F_*) + c \sum_{k=1}^{T-1} \alpha_k^2.$$

759 Therefore,

$$\mathbb{P}(\tau \leq T, \mathcal{E}_T) \leq \frac{F(\mathbf{w}_1) - F_* + c \sum_{k=1}^{T-1} \alpha_k^2}{B}.$$

760 Finally,

$$\mathbb{P}(\tau > T) \geq 1 - \mathbb{P}(\tau \leq T, \mathcal{E}_T) - \mathbb{P}(\mathcal{E}_T^c) \geq 1 - \frac{F(\mathbf{w}_1) - F_* + c \sum_{k=1}^{T-1} \alpha_k^2}{B} - \sum_{k=1}^{T-1} \delta_k,$$

761 and truncation gives the $\max\{0, \cdot\}$ form. \square

762 D Numerical experiments

763 D.1 Implementation details

764 The algorithms in this paper were implemented in Python using `jax` (version 0.5.0), `flax` (version 0.10.0),
 765 and `optax` (version 0.2.4). All timing results reported in Section 4 were measured on a consistent hardware
 766 platform running Ubuntu 24.04.2 LTS, equipped with an Intel(R) Core(TM) i7-12700K CPU (8 Performance-
 767 cores @ 3.60 GHz and 4 Efficient-cores @ 2.70 GHz), and 64 GB of system memory. All experiments were
 768 executed in double precision arithmetic to ensure numerical stability for the challenging SciML problems.

769 D.2 Baseline methods and experimental setting

770 Our experiments evaluated several optimization algorithms to validate our theoretical analysis of precon-
 771 ditioning effects. We implemented vanilla SGD, SGD with momentum ($\beta = 0.9$), and the preconditioned
 772 methods using GGN and Hessian approximations. The preconditioned methods employ conjugate gradient to
 773 efficiently approximate matrix-vector products with the inverse preconditioner, avoiding the prohibitive cost
 774 of explicitly forming and inverting the full matrices. This approach provides a computationally tractable way
 775 to incorporate curvature information into the optimization process. For Adam (with $\beta_1 = 0.9$, $\beta_2 = 0.999$)
 776 and L-BFGS (with memory size 100 and maximum line search of 100 steps), we utilized the implementations
 777 available in the `optax` library.

778 Our experimental protocol employed a structured two-phase optimization strategy. Phase I utilized Adam
 779 with a learning rate of 0.001 until convergence slowed significantly. This established a common starting
 780 point in the optimization landscape and helped navigate past initial high-gradient regions. In Phase II, we
 781 transitioned to the respective optimization methods for direct performance comparison. The specific duration
 782 of each phase varied by task complexity and is detailed in the respective experimental sections.

783 We individually optimized learning rates for each method-task combination through grid search, deliberately
 784 omitting learning rate schedulers to isolate the inherent convergence properties of each optimizer. For
 785 Adam, we searched within the range $\{0.001, 0.0005, 0.0002, 0.0001, \dots, 0.00001\}$. The preconditioned methods
 786 required different learning rate ranges due to their curvature properties: CG-Hessian and CG-GGN used
 787 $\{1.0, 0.5, \dots, 0.001\}$. This difference reflects our theoretical analysis that effective preconditioning can support
 788 larger learning rates when operating near local minima. For vanilla SGD and momentum SGD, we initially
 789 explored the same ranges as Adam and expanded to wider intervals when necessary to ensure optimal
 790 performance. This methodology ensured a fair comparison by allowing each optimizer to operate at its most
 791 effective learning rate for each specific task.

792 To ensure robust experimental results, we conducted each experiment five times using different random
 793 seeds (42 to 46 for Phase I and 43 to 47 for Phase II). This approach accounts for the inherent stochasticity
 794 in neural network training processes and allows us to report mean performance metrics. For our timing
 795 analysis, we implemented a precise measurement protocol that isolates the computational efficiency of the
 796 optimization methods themselves. Specifically, we excluded all data generation and preprocessing overhead,
 797 capturing only the cumulative duration of the actual training iterations on identical hardware configurations.
 798 This methodology provides an equitable assessment of computational efficiency, particularly important
 799 when comparing methods with substantially different per-iteration costs, such as first-order methods versus
 800 preconditioned approaches that require conjugate gradient iterations.

801 **D.3 Noisy data regression**

802 For the Franke function regression experiment, we used a neural network with two hidden layers of 50 neurons
 803 each and ReLU activation functions. We resampled the dataset every epoch, generating 256 points with
 804 additive Gaussian noise as described in Appendix 4.2 and illustrated in the left panel of Figure 6. For the
 805 preconditioned methods, we employed 5 conjugate gradient iterations. The right panel of Figure 6 extends
 806 our main results by displaying not only the mean performance across 5 independent runs but also the variance
 807 bands for each optimization method.

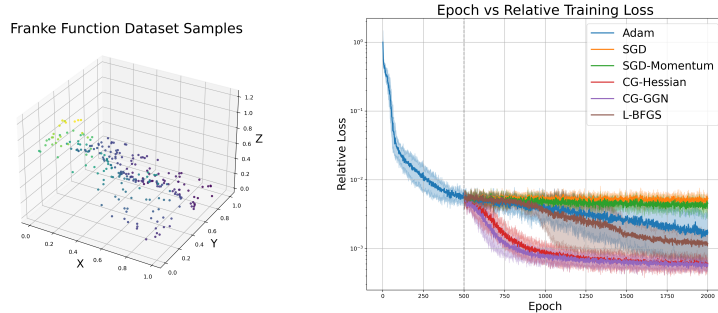


Figure 6: Left: Visualization of the Franke function dataset sampling. Right: Franke function regression performance averaged over 5 independent runs. Left: Training loss versus epochs with Phase I transitioning to Phase II at epoch 500 with variance.

808 **D.4 Physics-informed neural networks**

809 For solving the Poisson equation with PINNs, we used a neural network with two hidden layers of 50 neurons
 810 each and tanh activation functions. We resampled the dataset every epoch, generating 1,000 points within
 811 the domain and 200 points on the boundary, as described in Appendix 4.2 and illustrated in the left panel of
 812 Figure 7. For the preconditioned methods, we employed 20 conjugate gradient iterations. The right panel of
 813 Figure 7 shows that the mean loss trajectory is accompanied by a tight variance envelope across 5 independent
 814 runs.

815 **D.5 Green's function learning**

816 For both cases in the Green's function experiments, we used a neural network with five hidden layers of
 817 20 neurons each and tanh activation functions. We resampled the dataset every epoch, generating 1,000
 818 points within the domain, 500 points such that x is close to y , and 200 points on the boundary. For the
 819 preconditioned methods, we employed 20 conjugate gradient iterations. Figure 9 extends our main results by
 820 displaying not only the mean performance across 5 independent runs but also the variance bands for each
 821 optimization method.

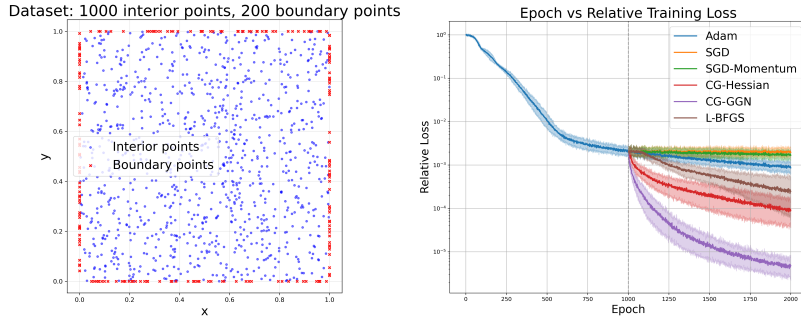


Figure 7: Left: Visualization of the sampling strategy for the 2D Poisson equation PINNs. The plot shows the distribution of 1,000 collocation points within the domain (blue) and 200 points along the boundary (red) used for enforcing the PDE and boundary conditions respectively. Right: Poisson equation PINNs performance averaged over 5 independent runs. Training loss versus epochs with Phase I transitioning to Phase II at epoch 1,000 with variance.

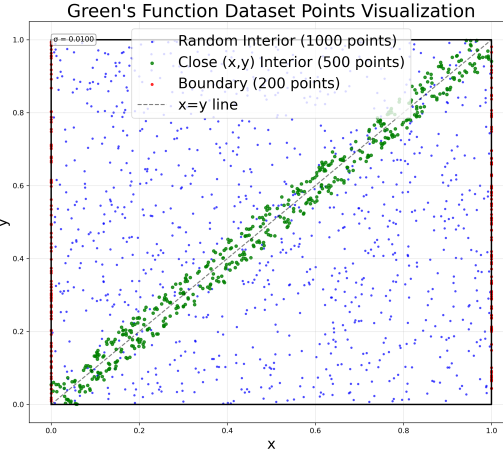


Figure 8: Visualization of the sampling strategy for Green's function learning. The plot shows three categories of training points: randomly distributed interior points (blue, 1,000 points), points concentrated near the diagonal where x is close to y (green, 500 points) to capture the near-singularity behavior characteristic of Green's functions, and boundary points (red, 200 points) used to enforce homogeneous Dirichlet boundary conditions.

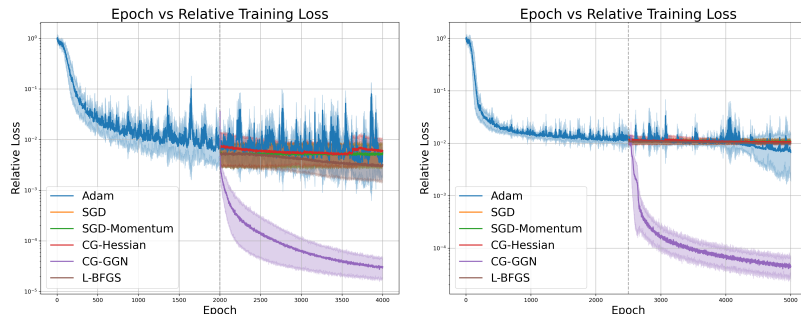


Figure 9: Green's function learning performance averaged over 5 independent runs. Left: Training loss versus epochs with Phase I transitioning to Phase II at epoch 2,000 with variance for Laplacian. Right: Training loss versus epochs with Phase I transitioning to Phase II at epoch 2,500 with variance for convection-diffusion.